

Non-equilibrium quantum transport through a dissipative resonant level

Chung-Hou Chung^{1,2}, Karyn Le Hur^{3,4}, Gleb Finkelstein⁵, Matthias Vojta⁶, and Peter Wölfle^{7,8}

¹*Department of Electrophysics, National Chiao-Tung University, HsinChu, Taiwan, R.O.C.*

²*Physics Division, National Center for Theoretical Sciences, HsinChu, Taiwan, R.O.C.*

³*Center for Theoretical Physics Ecole Polytechnique and CNRS 91128 Palaiseau, France*

⁴*Department of Physics and Applied Physics, Yale University, New Haven, CT, USA*

⁵*Department of Physics, Duke University, Durham, NC 27708, U.S.A.*

⁶*Institut für Theoretische Physik, Technische Universität Dresden, 01062 Dresden, Germany*

⁷*Institut für Theorie der Kondensierten Materie, KIT, 76128 Karlsruhe, Germany*

⁸*Institut für Nanotechnologie, KIT, 76021 Karlsruhe, Germany*

(Dated: August 14, 2018)

The resonant-level model represents a paradigmatic quantum system which serves as a basis for many other quantum impurity models. We provide a comprehensive analysis of the non-equilibrium transport near a quantum phase transition in a spinless dissipative resonant-level model, extending earlier work [Phys. Rev. Lett. **102**, 216803 (2009)]. A detailed derivation of a rigorous mapping of our system onto an effective Kondo model is presented. A controlled energy-dependent renormalization group approach is applied to compute the non-equilibrium current in the presence of a finite bias voltage V . In the linear response regime $V \rightarrow 0$, the system exhibits as a function of the dissipative strength a localized-delocalized quantum transition of the Kosterlitz-Thouless (KT) type. We address fundamental issues of the non-equilibrium transport near the quantum phase transition: Does the bias voltage play the same role as temperature to smear out the transition? What is the scaling of the non-equilibrium conductance near the transition? At finite temperatures, we show that the conductance follows the equilibrium scaling for $V < T$, while it obeys a distinct non-equilibrium profile for $V > T$. We furthermore provide new signatures of the transition in the finite-frequency current noise and AC conductance via the recently developed Functional Renormalization Group (FRG) approach. The generalization of our analysis to non-equilibrium transport through a resonant level coupled to two chiral Luttinger-liquid leads, generated by the fractional quantum Hall edge states, is discussed. Our work on dissipative resonant level has direct relevance to the experiments in a quantum dot coupled to resistive environment, such as H. Mebrahtu *et al.*, Nature **488**, 61, (2012).

PACS numbers: 72.15.Qm, 73.23.-b, 03.65.Yz

I. INTRODUCTION

Quantum phase transitions (QPTs)^{1,2} which separate competing ground states represent generic phenomena in solid-state systems at zero temperature. The transition is frequently found to be continuous, often times giving rise to a quantum critical point. In the neighborhood of a quantum critical point of a metallic system the finite temperature properties as a rule show non-Fermi liquid behavior³. In recent years, quantum phase transitions at the nanoscale have attracted much attention^{4–15}. Much of the effort has been focused on the breakdown of the Kondo effect in transport of a quantum dot due to its coupling to a dissipative environment. However, relatively less is known about the corresponding out-of-equilibrium properties^{16–23,25?}. A finite bias voltage applied across a nanosystem is expected to smear out the equilibrium transition, but the current-induced decoherence might act quite differently as compared to thermal decoherence at finite temperature T , resulting in exotic behavior near the transition.

Meanwhile, understanding the interplay of electron interactions and non-equilibrium effects in quantum systems is one of the most challenging open questions in condensed matter physics. Many of the theoretical ap-

proaches that have been proven so successful in treating strongly correlated systems in equilibrium are simply inadequate once the system is out of equilibrium. The real-time Schwinger-Keldysh formalism²⁶ has been known as the most successful approach to non-equilibrium dynamics since it offers a controlled perturbative expansion of the density operator. However, care must be taken to avoid the appearance of infrared divergences, in the perturbative approaches. Though much is known for quantum impurity systems in equilibrium, understanding their properties in non-equilibrium steady-state is still limited. Nevertheless, significant progress has been made by different approaches, such as (1) analytical approximations: perturbative renormalization group method (RG)^{27,28}, Hamiltonian flow equations²⁹, Functional RG^{30,31}, strong-coupling expansions³², master equations³³; (2) exact analytical solutions: field theory techniques³⁴, the scattering Bethe Ansatz³⁵, mapping of a steady-state non-equilibrium problem onto an effective equilibrium system³⁶; (3) numerical methods: time-dependent density matrix renormalization group (RG)³⁷, time-dependent numerical RG³⁸, diagrammatic Monte Carlo³⁹, and imaginary-time nonequilibrium quantum Monte Carlo⁴⁰.

In this paper, we provide a comprehensive analy-

sis of the non-equilibrium transport near a quantum phase transition in a dissipative resonant level model by employing the recently developed frequency-dependent RG²⁷ and Functional RG approaches³¹, and extending our earlier work in Ref. 16. We aim to address several fundamental questions related to the non-equilibrium transport in quantum dot settings, such as: what is the distinct non-equilibrium conductance profile at zero temperature compared to that in equilibrium at finite temperatures near the transition? is there any scaling behavior of the conductance at finite temperatures and finite bias voltage near the transition?

For this purpose, we investigate three classes of typical nano-models comprising a spinless resonant level coupled to: (i) two non-interacting Fermi-liquid leads subject to an Ohmic dissipative environment, where an Ohmic environment can be realized in a nanoscale resistor and has many applications in physics ranging from mesoscopic physics (Refs. 8,10,11) to biological systems⁴¹, (ii) two interacting fermion baths, in particular two Fractional Quantum Hall Edge (FQHE)⁴² leads, or the “chiral Luttinger liquids” where electrons on the edge of a 2D fractional quantum Hall system show one-dimensional chiral Luttinger liquid behaviors with only one species of electrons (left or right movers), (iii) two interacting Luttinger-liquid leads subject to an Ohmic dissipative environment.

In the class (i) model, the QPT separating the conducting and insulating phase for the level is solely driven by dissipation, which can be modeled by a bosonic bath. Dissipation-driven QPTs have been addressed theoretically and experimentally in various systems, such as: quantum dot systems^{9,43}, Josephson junction arrays^{44–46}, superconducting thin film^{47,48}, superconducting qubit⁴⁹, qubits or resonant level systems coupled to photonic cavities^{50,51}, and biological systems^{41,52}. Here, we focus on the non-equilibrium properties of the system near quantum phase transition. Meanwhile, for the class (ii) model, tunneling of electrons or quasi-particles between two FQHE states may in general suffer from the electron-electron interactions in FQHE. Interesting experimentally relevant questions arise regarding how interaction effects modify the nonequilibrium charge transport in such systems. Furthermore, one can extend the above two classes of models to a more general class (iii) model where both electron-electron interactions and the dissipation are present in the FQHE setups, which have not been explored both theoretically and experimentally. Our results have relevance for the recent experiment in Ref. 43 where the electronic transport through a resonant level in a nanotube exhibits the Luttinger liquid behavior, namely the conductance demonstrates a non-trivial power-law suppression as a function of bias voltage.

This paper is organized as follows: In Section II A, the model Hamiltonian of class (i) is introduced. In Section II B, we establish rigorous mappings of our model system, the class (i) model at a finite bias voltage, onto the out-of-equilibrium anisotropic Kondo model as well

as onto class (ii) and (iii) model systems subject to a finite voltage bias. We compute the current operator in Section II C for these three classes of models. We employ the nonequilibrium RG approach in Section III. Our results on nonequilibrium transport near the quantum phase transition both at zero and finite temperatures are presented in Section IV, followed by the results on the nonequilibrium finite-frequency current noise in Section V. We make a few remarks on the important issues of nonequilibrium quantum criticality in Section VI. Finally, we draw conclusions in Section VII.

II. MODEL HAMILTONIAN

A. Dissipative resonant level model

Our Hamiltonian in all of the three classes of models mentioned above takes the following generic form:

$$H = \sum_{k,i=1,2} [\epsilon(k) - \mu_i] c_{ki}^\dagger c_{ki} + t_i c_{ki}^\dagger d + h.c. \quad (1)$$

$$+ \sum_r \lambda_r (d^\dagger d - 1/2) (b_r + b_r^\dagger) + \sum_r \omega_r b_r^\dagger b_r,$$

where t_i is the (real-valued) hopping amplitude between the lead i and the quantum dot, c_{ki} and d are electron operators for the (Fermi-liquid type) leads and the quantum dot, respectively. $\mu_i = \pm V/2$ is the chemical potential shift applied on the lead i (V will denote the bias voltage throughout this paper), while the dot level is at zero chemical potential. Here, b_r are the boson operators of the dissipative bath with an Ohmic type spectral density⁸: $J(\omega) = \sum_r \lambda_r^2 \delta(\omega - \omega_r) = \alpha \omega$. Note that usually we introduce a cutoff via a $\exp(-\omega/\omega_c)$ function in $J(\omega)$; here, we assume that ω_c is a large energy scale comparable to the energy bandwidth of the reservoir leads. To simplify the discussion, we assume that the electron spins have been polarized through the application of a strong magnetic field. Note that our model can be realized experimentally in a quantum dot coupled to resistive environment as shown in Ref. 43.

In this section, we briefly summarize the behavior of our model system at equilibrium which means in the absence of a finite bias voltage ($V = 0$). A dissipative resonant-level systems in equilibrium coupled to several leads maps onto the anisotropic one-channel Kondo model^{8,10,11} where the dimensionless transverse Kondo coupling $g_\perp^{(e)}$ is proportional to the hopping t between the level and the leads and the longitudinal coupling $g_z^{(e)} \propto 1 - \sqrt{\alpha}$ (the exact prefactors are given in Refs. 8,10,11; see also Sec. II B and Appendix A). Here, the superscript (e) in $g_{\perp/z}^{(e)}$ refers to the equilibrium couplings. The model exhibits a Kosterlitz-Thouless (KT) QPT from a delocalized (Kondo screened) phase for $g_\perp^{(e)} + g_z^{(e)} > 0$, with a large conductance, $G \approx e^2/h$, to a localized (local moment) phase for $g_\perp^{(e)} + g_z^{(e)} \leq 0$,

with a small conductance, as the dissipation strength is increased (see Fig. 1). For $g_{\perp}^{(e)} \rightarrow 0$, the KT transition occurs at $\alpha_c = 1$. As $\alpha \rightarrow \alpha_c$, the Kondo temperature T_K obeys⁷: $\ln T_K \propto 1/(\alpha - \alpha_c)$. Note that here we assume our resonant level system exhibits the particle-hole (p-h) symmetry; namely, the resonant-level energy ϵ_d is set to be zero ($\epsilon_d = 0$). However, in a more general resonant-level model where p-h symmetry is absent, an additional term of the form $\epsilon_d d^{\dagger} d$ is present in the Hamiltonian Eq. (2). In terms of its equivalent Kondo model, this p-h symmetry breaking term plays the role as an effective local magnetic field $B_z \propto \epsilon_d$ acting on the impurity spin in the Kondo model¹¹, which needs more involved treatments and exceeds the scope of a simple and generic model system considered in the present work.

In equilibrium, the dimensionless scaling functions $g_{\perp}^{(e)}(T)$ and $g_z^{(e)}(T)$ at the transition are obtained via the renormalization-group (RG) equations of the anisotropic Kondo model:

$$g_{\perp,cr}^{(e)}(T) = -g_{z,cr}^{(e)}(T) = (2 \ln(\mathcal{D}/T))^{-1}, \quad (2)$$

where $\mathcal{D} = D_0 e^{1/(2g_{\perp})}$, with D_0 being the ultraviolet cutoff. Having in mind a quantum dot at resonance, $D_0 = \min(\delta\epsilon, \omega_c)$, with $\delta\epsilon$ being the level spacing on the dot and ω_c the cut-off of the bosonic bath; D_0 is of the order of a few Kelvins. At low temperatures $T \ll D_0$, the conductance drops abruptly with decreasing temperatures⁹:

$$G_{eq}(\alpha_c, T \ll D_0) \propto [g_{\perp,cr}^{(e)}(T)]^2 \propto \frac{1}{\ln^2(T/\mathcal{D})}. \quad (3)$$

Below, we analyze the non-equilibrium ($V \neq 0$) transport of our model system at the KT transition and in the localized phase in the double-barrier resonant tunneling regime where the dissipative resonant level couples symmetrically to the two leads ($t_1 = t_2 = t$). Note, however, that when the dissipative resonant level couples asymmetrically to the leads $t_1 \neq t_2$, as has been observed experimentally in Ref. 43, the system reaches the single-barrier tunneling regime, leading to Luttinger liquid behavior in conductance with power-law dependence in bias voltage.

For the sake of convenience, we set the following units throughout the rest of the paper: $e = \hbar = D_0 = k_B = 1$, and the temperature T is in unit of $D_0 = 1$.

B. Useful Mappings

Our generic model Hamiltonian Eq. (2) in fact can be mapped onto various related model systems as we shall discuss below, including the anisotropic Kondo model (class (i)), the class (ii) and (iii) systems mentioned above. Here, we will address the non-equilibrium transport through a dissipative resonant level based on one of

the equivalent models: the two-lead anisotropic Kondo model. The mappings for the three classes of models discussed below will be derived in an analogous way. The general scheme of these mappings is via bosonization followed by re-fermionization (or in the opposite order)^{53,54}.

1. Mapping the dissipative resonant level model onto the anisotropic Kondo model

First, we envision a non-equilibrium mapping revealing that the leads are controlled by distinct chemical potentials. Through similar bosonization and refermionization procedures as in equilibrium, our model is mapped onto an anisotropic Kondo model^{7,8,10,11} with the effective (Fermi-liquid) left (L) and right lead (R)⁵⁶ (see Appendix A for details):

$$\begin{aligned} H_K = & \sum_{k,\gamma=L,R,\sigma=\uparrow,\downarrow} [\epsilon_k - \mu_{\gamma}] c_{k\gamma\sigma}^{\dagger} c_{k\gamma\sigma} \\ & + (J_{\perp}^{(1)} s_{LR}^{+} S^{-} + J_{\perp}^{(2)} s_{RL}^{+} S^{-} + h.c.) \\ & + \sum_{\gamma=L,R} J_z s_{\gamma\gamma}^{z} S^z, \end{aligned} \quad (4)$$

where $c_{kL(R)\sigma}^{\dagger}$ is the electron operator of the effective lead $L(R)$, with σ the spin quantum number, $\gamma = L, R$ is the index for the effective non-interacting fermionic leads, $S^{+} = d^{\dagger}$, $S^{-} = d$, and $S^z = Q - 1/2$ where $Q = d^{\dagger} d$ describes the charge occupancy of the level. Additionally, $s_{\gamma\beta}^{\pm} = \sum_{\alpha,\delta,k,k'} \frac{1}{2} c_{k\gamma\alpha}^{\dagger} \sigma_{\alpha\delta}^{\pm} c_{k'\beta\delta}$ are the spin-flip operators between the effective leads γ and β , $J_{\perp}^{(1),(2)} \propto t_{1,2}$ embody the transverse Kondo couplings, $J_z \propto (1 - 1/\sqrt{2\alpha^*})$, and $\mu_{\gamma} = \pm \frac{V}{2} \sqrt{1/(2\alpha^*)}$. It should be noted that this mapping is exact near the phase transition where $\alpha \rightarrow 1$ or $\alpha^* \equiv \frac{1}{1+\alpha} \rightarrow 1/2$, and thus $\mu_{\gamma} = \pm V/2$. Note that the above mapping takes a spinless dissipative resonant level model with spinless fermionic baths $c_{\alpha=1,2}$ to the anisotropic Kondo model with a “spinful” quantum dot (with spin operator given by $S^{+,-,z}$) and “spinful” conduction electron leads $\tilde{c}_{\gamma=L,R}^{\sigma}$. The appearance of the “pseudo-spin” degrees of freedom in the effective Kondo model can be understood in terms of the “charge Kondo” effect: the the tunneling between a resonant level (which can be represented by a “qubit” or a “spin”) and the spin-polarized leads plays an equivalent role as the “pseudo-spin” flips between spin of a quantum dot and that of the conduction electrons; and the coupling of the charge of the resonant level to the bosonic environment acts as the Ising coupling between z-components of the pseudo-spins on the dot and in the effective leads^{7,8}. Meanwhile, as mentioned above, when the resonant-level model shows p-h asymmetry, an additional term $\epsilon_d d^{\dagger} d$ appears in the Hamiltonian, which is equivalent to a local magnetic field acting on the impurity spin $\epsilon_d d^{\dagger} d \rightarrow B_z S_z$ via the identification: $d^{\dagger} = S^{+}$, $d = S^{-}$, and $d^{\dagger} d - 1/2 = S_z$. For

simplicity, we do not intend to study further this p-h asymmetry term and focus mainly on the effective Kondo model in the absence of magnetic field. Note also that the mapping has been derived earlier in Ref. 16 and is well-known at equilibrium (Ref. 8). In Appendix A, we will provide more details regarding the different theoretical steps, in particular with a finite bias voltage.

2. Mapping for a resonant level coupled to a FQHE

Our analysis for the non-equilibrium transport of a dissipative resonant level model is applicable for describing a resonant level quantum dot coupled to two chiral Luttinger liquid leads, which is relevant for describing quasi-particle tunneling between two Fractional Quantum Hall Edge (FQHE) states⁴² (the class (ii) model mentioned above). In the absence of bias voltage, this case has been studied in Refs. 8,11. Via the standard bosonization,

$$c_\alpha(0) = \frac{1}{\sqrt{2\pi a}} F_\alpha e^{i\frac{\varphi_\alpha(0)}{K}}, \quad (5)$$

the Hamiltonian of such system can be written as^{7,8,11,42} (see Appendix A.):

$$H_{FQHE} = H_{chiral} + H_t + H_\mu, \quad (6)$$

where the lead term H_{chiral} describes two chiral Luttinger liquid leads with lead index $\alpha = 1, 2$, H_t denotes the tunneling term and the bias voltage term H_μ is given respectively by:

$$\begin{aligned} H_{chiral} &= \frac{1}{2} \int_{-\infty}^{+\infty} \sum_{\alpha=1,2} \left(\frac{d\varphi_\alpha}{dx} \right)^2 dx, \\ H_t &= t_1 e^{i\varphi_1/\sqrt{K}} d + t_2 e^{i\varphi_2/\sqrt{K}} d + h.c. \\ H_\mu &= -\frac{V}{2} \frac{1}{\sqrt{K}} (\partial\varphi_1 - \partial\varphi_2), \end{aligned} \quad (7)$$

where the boson field $\varphi_{\alpha=1,2}$ denotes the chiral Luttinger liquid in lead α , the tunneling between lead and the resonant level is given by t_α , V is the bias voltage, and K refers to the Luttinger parameter. Here, we set $2\pi a = 1$ throughout the paper with a being the lattice constant. Through the similar refermionization, we arrive at the effective Kondo model as shown in Eq. (4) with the bare Kondo couplings $J_\perp^{(1),(2)} = t e^{i(\sqrt{2} - \frac{1}{\sqrt{K}})\varphi_{2,1}}$, $J_z = 1 - 1/\sqrt{2K}$. The non-equilibrium RG scaling equations for H_{FQHE} have the same form as in Eq. (14).

3. Mapping for a dissipative resonant level coupled to interacting leads

So far, we consider here just a dissipative resonant single-level coupled to two non-interacting leads. Nev-

ertheless, the mapping can be straightforwardly generalized to the same system but with a spinless quantum dot which contains many energy levels. In this case, the effective Luttinger liquid parameter K' is modified as: $\frac{1}{K'} = \frac{1}{K} + 1$ (see Eq. (A22) in Appendix A). More generally, the mapping can be further generalized to the system of a many-level (single-level) spinless quantum dot with Ohmic dissipation coupled to two chiral Luttinger liquid leads with Luttinger parameter K , giving rise to the effective Luttinger liquid parameter \tilde{K} defined as (see Eq. (A24) in Appendix A):

$$\tilde{K} = \frac{1}{K} + 1 + K_b \quad (8)$$

for a many-level spinless quantum dot and

$$\frac{1}{\tilde{K}} = \frac{1}{K} + K_b \quad (9)$$

for a spinless quantum dot with a single resonant level. Details of the mapping is given in Appendix A.

C. Average current

We may compute the non-equilibrium current operator in the effective models through the mappings. We will first compute the current operator within the effective anisotropic Kondo model as it is the main focus of this paper. From the mapping described in Sec. II. B 1., we can establish the invariance of the net charge on the resonant level upon the mapping: $N_1 - N_2 = N_L - N_R$, where $N_i = \sum_{ki} c_{ki}^\dagger c_{ki}$ represents the charge in lead $i = 1, 2$, whereas $N_\gamma = \sum_k c_{k\gamma\sigma}^\dagger c_{k\gamma\sigma}$ represents the charge in the effective lead $\gamma = L, R$. This allows us to check that the averaged currents within the Keldysh formalism²⁶ are the same in the original and in the effective Kondo model (see Appendix B for details):

$$\begin{aligned} I &= i[Q_L - Q_R, H_K] \\ &= iJ_\perp^{(1)}(s_{LR}^- S^+ - s_{RL}^+ S^-) - (1 \rightarrow 2, L \rightarrow R). \end{aligned} \quad (10)$$

Thus, the current I can be computed from the Kondo model due to the invariance of the average current upon the mapping mentioned above. Note that through the various mappings mentioned above, it is straightforward to see that the current operator for other related models—resonant level coupled to FQHE leads and dissipative resonant level (both small and large in size) coupled to interacting Luttinger liquid leads—take exactly the same form as shown in Eq. (10).

III. NON-EQUILIBRIUM RG APPROACH

A. RG equations

Now, we employ the non-equilibrium RG approach to the effective Kondo model²⁷ in Eq. (4). In this ap-

proach, the Anderson's poor-man scaling equations are generalized to non-equilibrium RG equations by including the frequency dependence of the Kondo couplings and the decoherence due to the steady-state current at finite bias voltage²⁷. For the sake of simplicity, we assume that the resonant level (quantum dot) is symmetrically coupled to the right and to the left lead, $t_1 = t_2$ (or $J_{\perp}^{(1)} = J_{\perp}^{(2)} \equiv J_{\perp}$). We will discuss in Appendix C the more general case with $t_1 \neq t_2$. The dimensionless Kondo couplings as a function of frequency ω exhibit an extra symmetry due to the particle-hole symmetry of the effective Kondo model: $g_{\perp(z)}(\omega) = g_{\perp(z)}(-\omega)$ where $g_{\perp(z)}(D_0) = N(0)J_{\perp(z)}$ is the initial value, with $N(0)$ being the density of states per spin of the conduction electrons. Here, we suppress the upper script symbol ^(e) in the Kondo couplings since we will now focus on the non equilibrium case V not zero. We obtain²⁷:

$$\begin{aligned} \frac{\partial g_z(\omega)}{\partial \ln D} &= - \sum_{\beta=-1,1} \left[g_{\perp} \left(\frac{\beta V}{2} \right) \right]^2 \Theta_{\omega + \frac{\beta V}{2}}, \\ \frac{\partial g_{\perp}(\omega)}{\partial \ln D} &= - \sum_{\beta=-1,1} g_{\perp} \left(\frac{\beta V}{2} \right) g_z \left(\frac{\beta V}{2} \right) \Theta_{\omega + \frac{\beta V}{2}}, \end{aligned} \quad (11)$$

where $\Theta_{\omega} = \Theta(D - |\omega + i\Gamma|)$, $D < D_0$ is the running cutoff. Here, Γ is the decoherence (dephasing) rate at finite bias which cuts off the RG flow²⁷. In the Kondo model, Γ corresponds to the relaxation rate due to spin flip processes (which are charge flips in the original model), defined as the broadening $\Gamma = \Gamma_s$ of the dynamical transverse spin susceptibility $\chi^{\perp}(\omega)$ in the effective Kondo model⁵⁷:

$$\chi^{\perp}(\omega) = \chi_0 \frac{i\Gamma_s}{\omega + i\Gamma_s} \quad (12)$$

with $\chi^{\perp}(\omega)$ being the time Fourier transform of the spin susceptibility $\chi^{\perp}(t) = i\theta(t)\langle [S^-(t), S^+(0)] \rangle = i\theta(t)\langle [f_{\downarrow}^{\dagger}(t)f_{\uparrow}(t), f_{\uparrow}^{\dagger}(0)f_{\downarrow}(0)] \rangle$, and χ_0 being $\chi^{\perp}(\omega = 0)$. Here, we take the pseudo-fermion representation of the spin operators $S^{+,-,z} = \frac{1}{2}f_{\alpha}\sigma_{\alpha\beta}^{+,-,z}f_{\beta}$ with $f_{\sigma=\uparrow,\downarrow}$ being the pseudo-fermion operator and $\sigma^{+,-,z}$ being the Pauli matrices²⁷.

In the original model the decoherence rate Γ corresponds to the charge flip rates, defined as the broadening Γ_d of the resonant-level (d -electron) Green's function (or equivalently the imaginary part of the resonant-level self-energy $Im(\Sigma_d(\omega))$): $\Gamma = \Gamma_d = Im(\Sigma_d(\omega))$ where the self-energy $\Sigma_d(\omega)$ of the d -electron Green's function is defined via: $1/G_d(\omega) \propto \omega + \epsilon_d + Re(\Sigma_d(\omega)) + iIm(\Sigma_d(\omega))$ with $G_d(\omega)$ being the Fourier transform of the resonant-level Green's function $G_d(t) = i\theta(t)\langle [d(t), d^{\dagger}(0)] \rangle$. These two definitions for Γ agree with each other with the proper identification: $d = S^-$, $d^{\dagger} = S^+$.

Note that these RG equations in the present context were already discussed in the short Ref. 16, but now we will elaborate the methodology. The configurations of

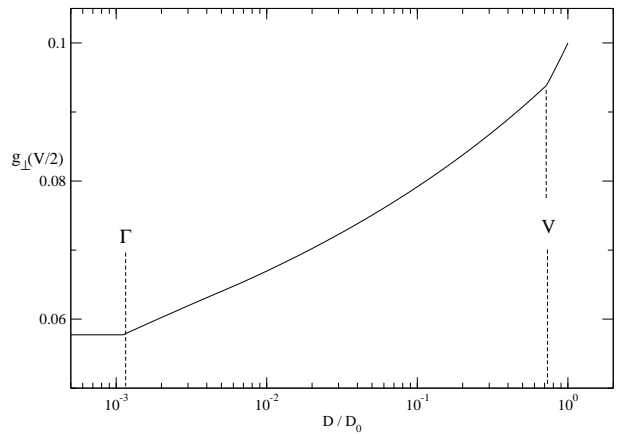


FIG. 1: RG flow of $g_{\perp,cr}(V/2)$ at the transition as a function of bandwidth cutoff D (in unit of D_0); the bare couplings are $g_{\perp} = -g_z = 0.1$ (in unit of D_0). We have set $V = 0.72$ (in unit of D_0). The decoherence rate Γ is around $0.00117D_0$.

the system out of equilibrium are not true eigenstates, but acquire a finite lifetime. The spectral function of the fermion on the level is peaked at $\omega = \pm V/2$, and therefore we have $g_{\perp(z)}(\omega) \approx g_{\perp(z)}(\pm V/2)$ on the right hand side of Eq. (11). Other Kondo couplings are not generated. From Ref. 27 via the Fermi's golden rule of the spin-flip rates Γ in the Kondo model, we identify:

$$\begin{aligned} \Gamma &= \frac{\pi}{4} \sum_{\gamma, \gamma', \sigma} \int d\omega \left[n_{\sigma} g_z^2(\omega) f_{\omega - \mu_{\gamma}} (1 - f_{\omega - \mu_{\gamma'}}) \right. \\ &\quad \left. + n_{\sigma} g_{\perp}^2(\omega) f_{\omega - \mu_{\gamma}} (1 - f_{\omega - \mu_{\gamma'}}) \right], \end{aligned} \quad (13)$$

where f_{ω} is the Fermi function. Here, $\gamma = \gamma'$ for the $g_z^2(\omega)$ terms while $\gamma \neq \gamma'$ for the $g_{\perp}^2(\omega)$ terms with γ, γ' being L or R . We have introduced the occupation numbers n_{σ} for up and down spins satisfying $n_{\uparrow} + n_{\downarrow} = 1$ and $S_z = (n_{\uparrow} - n_{\downarrow})/2$. In the delocalized phase, we get $n_{\uparrow} = n_{\downarrow} = 1/2$, in agreement with the quantum Boltzmann equation²⁷. At the KT transition, we can use that $g_{\perp}(\omega) = -g_z(\omega)$ from the symmetry of the Kondo model and that $\sum_{\sigma} n_{\sigma} = 1$. Finally in the localized phase, we have $g_{\perp} \leq -g_z$, and n_{σ} satisfies $|S_z| \rightarrow 1/2$ (see Refs. 7,8,10,11), which remains true at a finite bias voltage.

B. Solutions to RG equations

Following the scheme of Ref. 27, we solve Eqs. (11) and (13) self-consistently. First, we compute $g_{\perp(z)}(\omega = \pm V/2)$ for a given cutoff D . We then substitute the solutions back into the RG equations to get the general solutions for $g_{\perp(z)}(\omega)$ at finite V , and finally extract the solutions in the limit $D \rightarrow 0$. When the cutoff D is lowered, the RG flows are not cutoff by V but they continue to flow for $\Gamma < D < V$ until they are stopped for $D \leq \Gamma$.

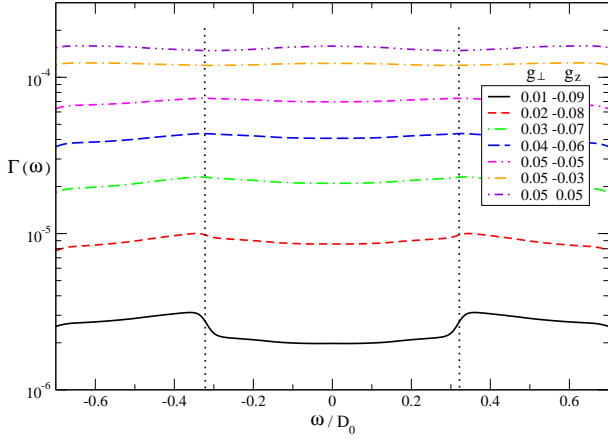


FIG. 2: (Color online) $\Gamma(\omega)$ at $T = 0$ versus ω across the KT transition. The bias voltage is fixed at $V = 0.32D_0$. $\Gamma(\omega)$ develops a peak (dip) at $\omega = 0$ in the delocalized (localized) phase, respectively. At $\omega \approx \pm V$ (vertical dotted lines), $\Gamma(\omega)$ shows peaks (for localized phase) or dips (for delocalized phase). Note that $\Gamma(\omega)$ weakly depends on ω for $|\omega| < V$, $\Gamma(|\omega| < V) \approx \Gamma(\omega = 0)$.

In Fig.1 we show a typical RG flow of $g_{\perp}(V/2)$ at the KT transition as a function of bandwidth D with the analytical approximation: $g_{\perp}(V/2) \approx \frac{1}{2 \ln \frac{D}{V}}$ for $D > V$, $g_{\perp}(V/2) \approx \frac{1}{\ln \frac{D^2}{V}}$ for $\Gamma < D < V$, and $g_{\perp}(V/2) \approx \frac{1}{\ln \frac{D^2}{V}}$ for $D < \Gamma$. Here, $\mathcal{D} = D_0 e^{1/(2g_{\perp})}$, with D_0 being the ultraviolet cutoff, and D is the running cutoff scale set by the RG scaling equations for $g_{\perp/z}$. This clearly shows that the RG flow of $g_{\perp}(V/2)$ is stopped at Γ , a much lower energy scale than V .

Note that the charge (or pseudospin) decoherence rate Γ is a function of frequency, $\Gamma(\omega)$ in the more general and rigorous Functional Renormalization Group (FRG) framework³¹. Here, $\Gamma = \Gamma(\omega = 0)$ within FRG. Nevertheless, we find $\Gamma(|\omega| \leq V)$ at $T = 0$ depends weakly on ω and can be well approximated by its value at $\omega = 0$, $\Gamma(T = 0, \omega) \approx \Gamma(T = 0, \omega = 0)$ (see Fig. 2). We have checked that the non-equilibrium current $I(V, T = 0)$ and conductance $G(V, T = 0)$ obtained from this approximation ($\Gamma(T = 0, \omega) \approx \Gamma(T = 0, \omega = 0)$) agrees very well with that from the more rigorous FRG approach based on the frequency-dependent decoherence rate $\Gamma(T = 0, \omega)$ (see Eq. (36) below) as a consequence of the fact that the current and conductance are integrated quantities over the frequencies, and they are insensitive to weak frequency-dependence of Γ . In Fig. 3 we show the RG flow of the decoherence rate $\Gamma(\omega = 0)$ as a function of D , using the same parameter as in Fig. 1. One observes that Γ tends to a finite value as $D \rightarrow 0$. The inset shows Γ as a function of V (see also section VI). Note that, unlike the equilibrium RG at finite temperatures where RG flows are cutoff by temperature T , here in non-equilibrium the RG flows will be cutoff by the decoherence rate Γ , an energy scale typically much

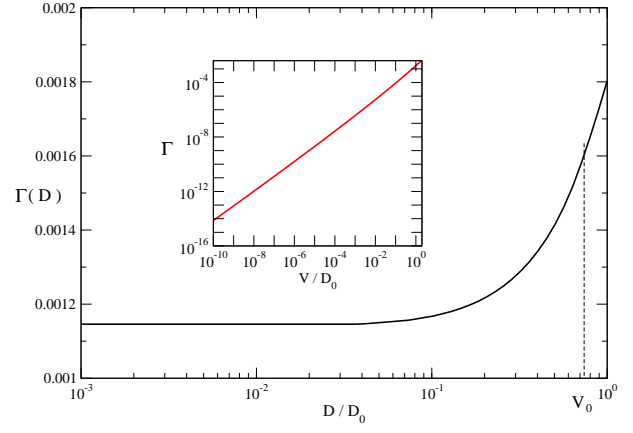


FIG. 3: (Color online) RG flow of $\Gamma(D)$ at $T = 0$ versus D (in unit of D_0) at a fixed bias voltage $V_0 = 0.72D_0$ (vertical dashed line) at the KT transition with bare Kondo couplings $g_{\perp} = 0.1 = -g_z$. Under RG, Γ approaches a constant value as $D \rightarrow 0$: $\Gamma(D \rightarrow 0) \approx 0.00117D_0$. Inset: Γ as a function of V for the same bare Kondo couplings.

higher than T , but much lower than V , $T \ll \Gamma \ll V$. Moreover, $\Gamma(V)$ is a non-linear function in V . (For example, at the KT transition, $\Gamma_{KT}(V) \propto V/[\ln(\frac{D}{V})]^2$.) The unconventional properties of $\Gamma(V)$ lead to a non-equilibrium conductance ($G(V, T = 0)$) distinct from that in equilibrium ($G(T, V = 0)$) near the KT transition¹⁶. In contrast, the equilibrium RG will lead to approximately frequency independent couplings, (or “flat” functions $g_{\perp}(\omega) \approx g_{\perp,z}(\omega = 0)$).

Notice that the mapping mentioned above works near the KT transition, $\alpha^* \equiv \frac{1}{1+\alpha} \rightarrow 1/2$. However, for a general case deep in the localized phase, the effective Kondo couplings acquire an additional phase $J_{\perp}^{(1),(2)} \propto t_{1,2} e^{i(\sqrt{2} - \frac{1}{\sqrt{K}})\tilde{\phi}_{s;2,1}}$ where the more general form of $J_{\perp}^{(1),(2)}$ and its phase $\tilde{\phi}_{s;2,1}$ are derived and defined in Eq. (A10) of Appendix A.. This results in a nonzero bare scaling dimension⁵³ for $J_{\perp}^{(1),(2)}$, $[J_{\perp}^{(1),(2)}] = \frac{1}{2}(\sqrt{2} - \frac{1}{\sqrt{K}})^2 = 1 - \sqrt{\frac{2}{K}} + \frac{1}{2K}$. This slightly modifies the non-equilibrium RG scaling equations to the following form:

$$\begin{aligned} \frac{\partial g_z(\omega)}{\partial \ln D} &= - \sum_{\beta=-1,1} \left[g_{\perp} \left(\frac{\beta V}{2} \right) \right]^2 \Theta_{\omega + \frac{\beta V}{2}} \\ \frac{\partial g_{\perp}(\omega)}{\partial \ln D} &= - \sum_{\beta=-1,1} \left[\frac{1}{2} \left(1 - \sqrt{\frac{2}{K}} + \frac{1}{2K} \right) g_{\perp} \left(\frac{\beta V}{2} \right) \right. \\ &\quad \left. + g_{\perp} \left(\frac{\beta V}{2} \right) g_z \left(\frac{\beta V}{2} \right) \right] \Theta_{\omega + \frac{\beta V}{2}} \end{aligned} \quad (14)$$

where the linear term $\frac{1}{2} \left(1 - \sqrt{\frac{2}{K}} + \frac{1}{2K} \right) g_{\perp} \left(\frac{\beta V}{2} \right)$ in Eq. (14) for $g_{\perp}(\omega)$ comes from the bare scaling dimension of $J_{\perp}^{(1),(2)}$ terms mentioned above, and it vanishes in the limit of $K \rightarrow 1/2$, as expected. In fact, this term applies

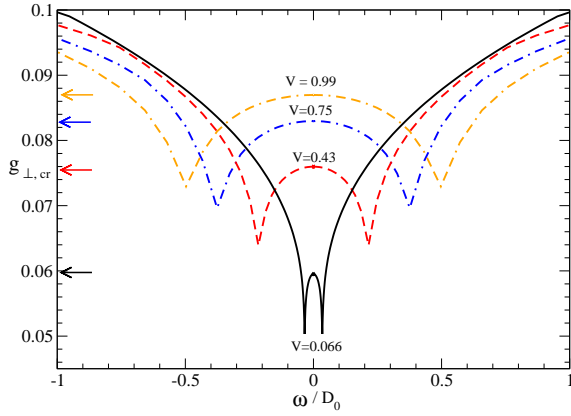


FIG. 4: $g_{\perp,cr}(\omega) = -g_{z,cr}(\omega)$ at the transition at various bias voltages V (in unit of D_0); the bare couplings are $g_{\perp} = -g_z = 0.1$ (in unit of D_0). The arrows give the values of $g_{\perp}(\omega = 0)$ at these bias voltages.

to the three models (case (i), (ii) and (iii)) through the mappings. Note that the above scaling equations may be cast in the same form as in Eq. (11) through redefinition of the coupling g_z : $g_z \rightarrow \bar{g}_z = g_z + \frac{1}{2}(1 - \sqrt{\frac{2}{K} + \frac{1}{2K}})$. All the previous results remain valid upon the above shift of g_z .

IV. NON-EQUILIBRIUM CONDUCTANCE

In the section, we present our results for non-equilibrium conductance. All explicit results will be obtained for the KT transition point and the localized phase, but not for the delocalized phase.

A. Non-equilibrium conductance at the KT transition

At the KT transition, we both numerically and analytically solve Eqs. (11) and (13) (in the limit of $D \rightarrow 0$). In particular, the approximated analytical solution within the approximation $\Theta_V \approx \Theta(D - V)$ due to $\Gamma \ll V$ is obtained:

$$g_{\perp,cr}(\omega) \approx \sum_{\beta} \Theta(|\omega - \beta V/2| - V) \frac{1}{4 \ln \left[\frac{D}{|\omega - \beta V/2|} \right]} \quad (15)$$

$$+ \Theta(V - |\omega - \beta V/2|) \times \left[\frac{1}{\ln[D^2/V \max(|\omega - \beta V/2|, \Gamma)]} - \frac{1}{4 \ln \frac{D}{V}} \right].$$

The solutions at the transition (denoted $g_{\perp,cr}$ and $g_{z,cr}$) are shown in Fig. 4. Since $g_{\perp,cr}(\omega)$ decreases under the RG scheme, the effect of the decoherence leads to minima; the couplings are severely suppressed at the points

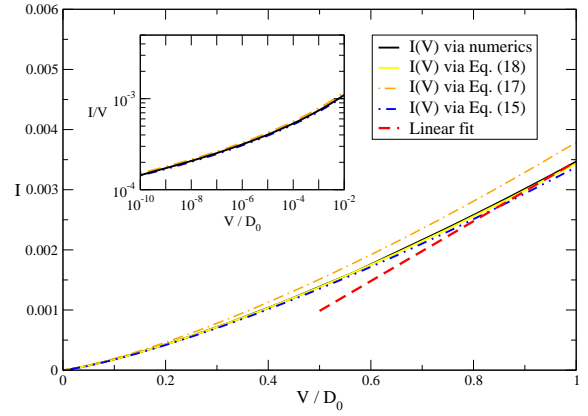


FIG. 5: Non-equilibrium current at the localized-delocalized transition. The naïve approximate analytical expression Eq. (17) fits well with the numerical result over several decades (from $V \approx 10^{-12}D_0$ to $V \approx 10^{-3}D_0$, see Inset). However, it starts to deviate from the numerical result at higher bias voltages.

$\omega = \pm \frac{V}{2}$. We also check that $g_{\perp,cr}(\omega) = -g_{z,cr}(\omega)$.

From the Keldysh calculation up to second order in the tunneling amplitudes, the current reads:

$$I = \frac{\pi}{8} \int d\omega \left[\sum_{\sigma} 4g_{\perp}(\omega)^2 n_{\sigma} \times \quad (16)$$

$$f_{\omega - \mu_L} (1 - f_{\omega - \mu_R}) \right] - (L \leftrightarrow R).$$

At $T = 0$, it simplifies as $I = \frac{\pi}{2} \int_{-V/2}^{V/2} d\omega g_{\perp}^2(\omega)$. Then, we numerically evaluate the non-equilibrium current. The differential conductance is obtained as $G(V) = dI/dV$. The $T = 0$ results at the KT transition are shown in Fig. 5 and Fig. 6.

First, it is instructive to compare the non-equilibrium current at the transition to the (naïve) approximation:

$$I_{cr} \approx \frac{\pi V}{2} [g_{\perp,cr}(\omega = 0)]^2 \approx \frac{\pi}{8} \frac{V}{(\ln^2(T_D/V))}. \quad (17)$$

As shown in Fig. 5, our numerically obtained non-equilibrium current fits well with the above analytical approximation for $V < 0.01D_0$. However, it starts to deviate from its numerically obtained values for higher bias voltages $V > 0.01D_0$. This deviation is due to the fact that the equilibrium form of the conductance at the transition is obtained by treating $g_{cr\perp}(\omega)$ a flat function within $-V/2 < \omega < V/2$: $g_{cr\perp}(\omega) \approx g_{cr\perp}(\omega = 0) \approx g_{cr\perp}^{eq}(T \rightarrow V)$. We have checked that the equilibrium coupling $g_{cr\perp}(\omega = 0)$ indeed corresponds to $g_{\perp}^{eq}(T = V)$, therefore the transport recovers the expected equilibrium form for $V \rightarrow 0$. However, since $g_{\perp}(\omega)$ is not a flat function for $-V/2 < \omega < V/2$ (it has two minima at $\omega = \pm V/2$), with increasing V (say for $V \approx 0.01D_0$) the non-equilibrium current exhibits a distinct behavior due to the frequency dependence of the coupling.

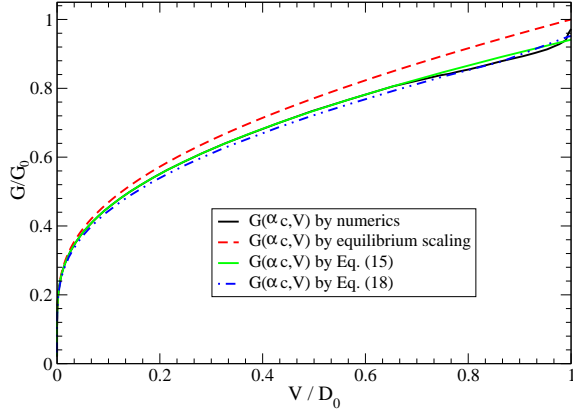


FIG. 6: Non-equilibrium conductance $G = dI/dV$ at the KT transition. G_0 is the equilibrium conductance at the transition for $T = D_0$: $G_0 = G_{eq}(\alpha_c, T = D_0) = 0.005\pi$ with the bare couplings $g_{\perp} = -g_z = 0.1D_0$.

In fact, the more accurate approximate expression for the non-equilibrium current at the transition is found to be:

$$I(\alpha_c, V) \approx \frac{\pi V}{2} \left(\frac{\pi}{4} [g_{\perp,cr}(\omega = 0)]^2 \right) + \frac{\pi V}{2} \left(\left(1 - \frac{\pi}{4}\right) [g_{\perp,cr}(\omega = V/2)]^2 \right), \quad (18)$$

where

$$g_{\perp,cr}(\omega = V/2) \approx 1/\ln\left(\frac{D^2}{\Gamma V}\right) \quad (19)$$

$$g_{\perp,cr}(\omega = 0) \approx 2 \left(\frac{1}{\ln(2D^2/V^2)} - \frac{1}{4\ln(D/V)} \right).$$

Here, we have treated $g_{\perp,cr}(\omega)^2$ within the interval $-V/2 < \omega < V/2$ as a semi-ellipse.

As demonstrated in Fig. 6, the conductance $G(V)$ obtained via the approximation in Eq. (18) fits very well with that obtained numerically over the whole range of $0 < V < D_0$. In the low-bias $V \rightarrow 0$ (equilibrium) limit, since $g_{\perp,cr}(\omega = 0) \approx g_{\perp,cr}^{(e)}(T = V) \ll 1$, we have $I(\alpha_c, V) \approx \frac{\pi V}{2} \left(g_{\perp,cr}^{(e)}(T = V) \right)^2$; therefore the scaling of $G(\alpha_c, V)$ is reminiscent of the equilibrium expression in Eq. (3), $G(\alpha_c, V) \approx \frac{\pi}{2} \left(g_{\perp,cr}^{(e)}(T = V) \right)^2 = \frac{\pi}{8} \frac{1}{\ln^2(D/V)}$. This agreement between equilibrium and non-equilibrium conductance at low V persists up to a crossover scale $V \approx 0.01D_0$ (determined for the parameters used in Fig. 6). At larger biases, the conductance shows a unique non-equilibrium profile; see Eq. (18). We find an excellent agreement of the non-equilibrium conductance obtained by three different ways — pure numerics, analytical solution Eq. (15) and the approximation in Eq. (18).

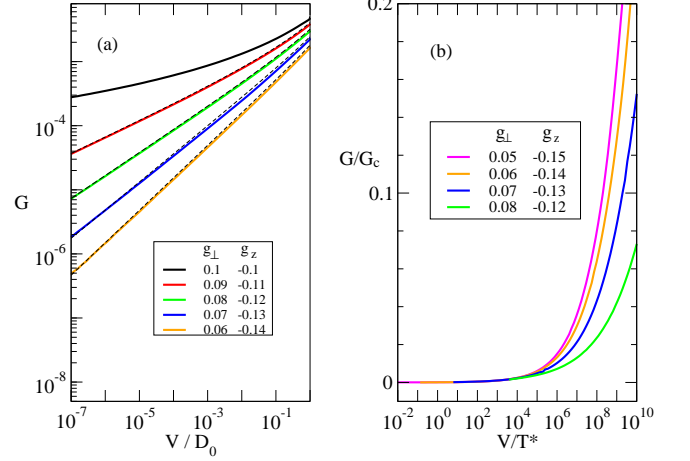


FIG. 7: Conductance in the localized phase (in units of π). (a) $G(V)$ at low bias follows the equilibrium scaling (dashed lines). (b) The conductance $G(V)/G_c$ is a function of V/T^* where we have defined $G_c = G(\alpha_c, V)$ and $T^* = D_0 e^{-\pi/\sqrt{g_z^2 - g_{\perp}^2}}$.

For large bias voltages $V \rightarrow D_0$, since $g_{\perp,cr}(\omega)$ approaches its bare value g_{\perp} , the non-equilibrium conductance increases rapidly and reaches $G(\alpha_c, V) \approx G_0 = \frac{\pi}{2} g_{\perp}^2$. Note that the non-equilibrium conductance is always smaller than the equilibrium one, $G(\alpha_c, V) < G_{eq}(\alpha_c, T = V)$, since $g_{\perp}(\omega = \pm V/2) < g_{\perp}(\omega = 0)$. Additionally, in the delocalized phase for $V \gg T_K > 0$, the RG flow of g_{\perp} is suppressed by the decoherence rate, and $G \propto 1/\ln^2(V/T_K)$ (Ref. 27).

B. Non-equilibrium conductance in the localized phase

In the localized phase, we first solve the equilibrium RG equations of the effective Kondo model analytically, resulting in

$$G_{loc}^{(e)}(T) = \frac{\pi}{2} \left(g_{\perp,loc}^{(e)}(T) \right)^2 \quad (20)$$

$$g_{\perp,loc}^{(e)}(T) = \frac{2cg_{\perp}(c + |g_z|)}{(c + |g_z|)^2 - g_{\perp}^2 \left(\frac{T}{D_0}\right)^{4c}} \left(\frac{T}{D_0}\right)^{2c} \quad (21)$$

where $c = \sqrt{g_z^2 - g_{\perp}^2}$. We introduce the energy scale $T^* = D_0 e^{-\pi/\sqrt{g_z^2 - g_{\perp}^2}}$ (which vanishes at the KT transition) such that $g_{\perp,loc}^{(e)}(T) \propto (T/T^*)^{2c}$ for $T \rightarrow 0$, leading to $G_{loc}^{(e)}(T) \propto (T/T^*)^{4c}$.

At a finite bias, we first solve for the self-consistent non-equilibrium RG equations both analytically and nu-

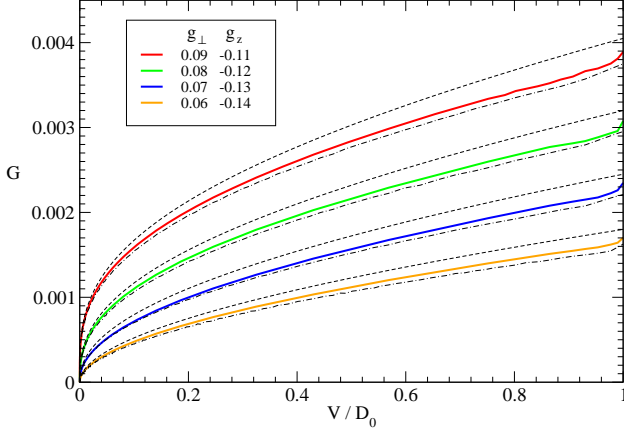


FIG. 8: Conductance in the localized phase (in units of π). At large bias voltages V , the non-equilibrium conductance $G(V)$ (solid lines) is distinct from the equilibrium form (dashed lines). The dot-dashed lines stem from an analytical approximation via Eq. (26).

merically, resulting in:

$$\begin{aligned}
 g_{\perp,loc}(\omega = V/2) &\approx g_{\perp} + \frac{A}{2c} [V^{2c} \sqrt{c^2 + A^2 V^{4c}}] \\
 &- \sqrt{A^2 + c^2} + \frac{B}{2c} [\Gamma^c \sqrt{c^2 + B^2 \Gamma^{2c}}] \\
 &- V^c \sqrt{c^2 + B^2 V^{2c}} \\
 &+ \frac{c}{2} \ln \left[\frac{B \Gamma^c + \sqrt{c^2 + B^2 \Gamma^{2c}}}{B V^c + \sqrt{c^2 + B^2 V^{2c}}} \right] \\
 &+ \frac{c}{2} \ln \left[\frac{A V^{2c} + \sqrt{c^2 + A^2 V^{4c}}}{A + \sqrt{c^2 + A^2}} \right],
 \end{aligned} \quad (22)$$

$$\begin{aligned}
 g_{\perp,loc}(\omega = 0) &\approx g_{\perp} + \frac{A}{2c} [V^{2c} \sqrt{c^2 + A^2 V^{4c}}] \\
 &- \sqrt{A^2 + c^2} + \frac{B}{c} \left[\left(\frac{V}{2}\right)^c \sqrt{c^2 + B^2 \left(\frac{V}{2}\right)^{2c}} \right] \\
 &- V^c \sqrt{c^2 + B^2 V^{2c}} \\
 &+ \frac{c}{2} \ln \left[\frac{B \left(\frac{V}{2}\right)^c + \sqrt{c^2 + B^2 \left(\frac{V}{2}\right)^{2c}}}{B V^c + \sqrt{c^2 + B^2 V^{2c}}} \right] \\
 &+ \frac{c}{2} \ln \left[\frac{A V^{2c} + \sqrt{c^2 + A^2 V^{4c}}}{[A + \sqrt{c^2 + A^2}]} \right],
 \end{aligned} \quad (23)$$

and similarly we get

$$\begin{aligned}
 g_{z,loc}(\omega = V/2) &\approx g_z + \frac{A^2}{2c} [1 - V^{4c}] \\
 &+ \frac{B^2}{2c} V^{2c} [1 - \left(\frac{\Gamma}{V}\right)^{2c}],
 \end{aligned} \quad (24)$$

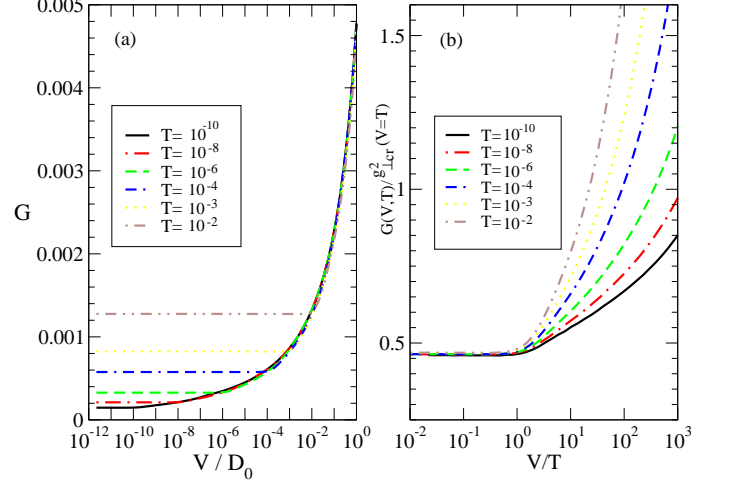


FIG. 9: Scaling of the conductance $G(V)$ at the KT transition (same unit as in Fig. 6). (a). For $V \gg T$, the conductance follows the non-equilibrium scaling $G(\alpha_c, V)$. (b). For $V < T$, now the conductance follows the equilibrium scaling $G_{eq}(\alpha_c, T)$.

$$\begin{aligned}
 g_{z,loc}(\omega = 0) &\approx g_z + \frac{A^2}{2c} [1 - V^{4c}] \\
 &+ \frac{B^2}{c} V^{2c} [1 - 2^{-2c}],
 \end{aligned} \quad (25)$$

where we unambiguously identify $A = \frac{g_{\perp}}{2} + \frac{c g_{\perp}}{c + |g_z|}$, $B = A V^c$; in this expression, V and Γ have been normalized to D_0 .

The non-equilibrium current in the localized phase $I_{loc}(V)$ is obtained via the same approximation leading to Eq. (19) at the KT transition:

$$\begin{aligned}
 I_{loc}(V) &\approx \frac{\pi V}{2} \left(\frac{\pi}{4} [g_{\perp,loc}(\omega = 0)]^2 \right) \\
 &+ \frac{\pi V}{2} \left(\left(1 - \frac{\pi}{4}\right) [g_{\perp,loc}(\omega = V/2)]^2 \right).
 \end{aligned} \quad (26)$$

As shown in Fig. 7, we numerically obtain the non-equilibrium conductance in the localized phase. For very small bias voltages $V \rightarrow 0$, we find that the conductance reduces to the equilibrium scaling: $G(V) \rightarrow G_{loc}^{(e)}(T = V) \propto (V/T^*)^{4c}$ (see Fig. 7 (a) and (b)). For $g_{\perp,loc} \ll |g_{z,loc}|$ and $\alpha^* = \frac{1}{1+\alpha} \rightarrow 1/2$, we get that the exponent $4c \approx 2\alpha^* - 1$, in perfect agreement with that obtained in equilibrium at low temperatures: $G(T) \propto T^{2\alpha^* - 1}$ (Ref. 9). At higher bias voltages $0.01 D_0 < V < D_0$, the conductance now follows a unique non-equilibrium form (consult Fig. 8) whose qualitative behavior is similar to that at the KT transition. Our non-equilibrium conductance obtained numerically in this phase is in very good agreement with that from the above approximated analytical solutions in Eq. 26 (see Fig. 8).

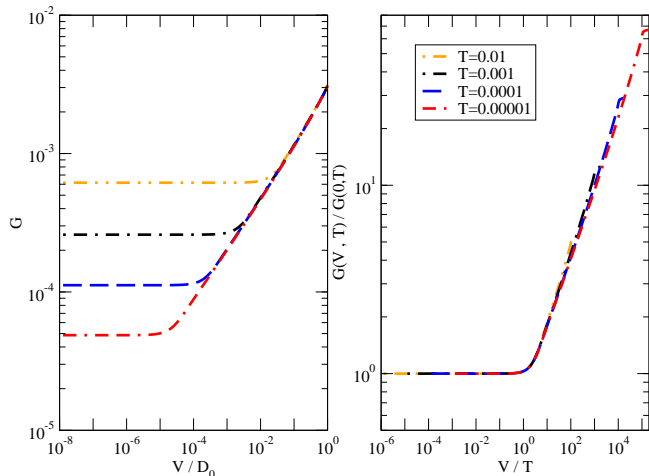


FIG. 10: Scaling of the conductance in the localized phase with $g_{\perp} = 0.08$, $g_z = -0.12$ (in unit of D_0). (a). For $V \gg T$, the conductance follows the non-equilibrium scaling $G(\alpha, V)$. (b). For $V \ll T$, now the conductance follows the equilibrium scaling $G_{eq}(\alpha_c, T)$.

C. Non-equilibrium conductance at finite temperatures

We have also analyzed the finite temperature profile of the non-equilibrium conductance at the transition and in the localized phase. We distinguish two different behaviors. At the KT transition, for $V > T$, the conductance $G(V, T)$ exhibits the same non-equilibrium form as $T = 0$, $G(V, T = 0)$ (see Fig. 9(a)); while as for $V < T$ it saturates at the value for the equilibrium conductance ($V = 0$) at finite temperatures (see Fig. 9(b)). In the localized phase, while for $V < T$ the conductance saturates at $G(V = 0, T)$ (Fig. 10(a)), for $V > T$, however, $G(V, T)$ exhibits universal power-law scaling:

$$G(V, T)/G(V = 0, T) \propto (V/T)^{4c} \quad (27)$$

(see Fig. 10(b)). This universal power-law scaling behavior in $G(V, T)$ looks qualitatively similar to that from the recent experiment on the transport through a dissipative resonant level in Ref. 43. However, these two power-law behaviors in conductance at a finite bias and temperature are different in their origins: The authors in Ref. 43 studied the quantum critical behavior of a dissipative resonant level in the regime of the delocalized phase ($\alpha < \alpha_c = 1$). As the resonant level is detuned from the Fermi level, the system at low temperatures exhibits power-law scaling in conductance at a large bias voltage $V > T$: $G(V/T) \propto (V/T)^{2\alpha}$ with $0 < \alpha < 1$. They showed further that this behavior is equivalent to that for a single-barrier tunneling of electrons through a Luttinger liquid. By contrast, the Luttinger-liquid-like power-law scaling in $G(V, T)$ (see Eq. (27)) we find here is the generic feature of a dissipative resonant level in the localized phase ($\alpha > \alpha_c = 1$), which has not yet

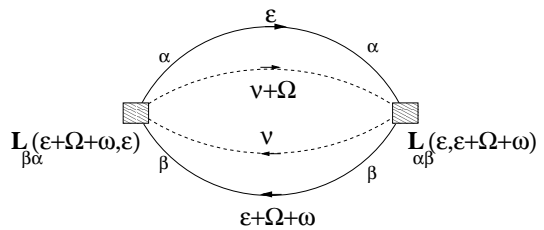


FIG. 11: (Color online) Diagram for the FF current noise $S(\omega)$. The solid lines represent conduction electron propagators; the dashed lines denote the pseudo-fermion propagators. The current vertex functions $L_{\alpha\beta}(\omega_1, \omega_2)$ are denoted by the shaded squares.

been explored experimentally. Therefore, our theoretical predictions on the nonequilibrium transport at a dissipative quantum phase transition offer motivations for further experimental investigations in the regime of our interest. The above two qualitatively different behaviors in conductance for $V < T$ and $V > T$ crossover at $V = T$. Note that similar behavior has been predicted in a different setup consisting of a magnetic Single Electron Transistor (SET) in Ref. 22 where a true quantum critical point separates the Kondo screened and the local moment phases.

V. NON-EQUILIBRIUM FINITE-FREQUENCY CURRENT NOISE

In addition to non-equilibrium current and conductance near the localized-delocalized transition addressed above, further insight on the phase transition can be obtained from the current fluctuations (or noise). The zero frequency shot noise has been used to probe the fractional charge of quasiparticle excitations in FQHE state tunnelings⁵⁹. However, even more useful information can be found in the finite-frequency (FF) current noise, which can be used to probe the crossover between different quantum statistics of the quasiparticles⁶⁰. Recently, there has been theoretical studies on the FF current noise of a non-equilibrium Kondo dot^{61–63}. So far, these studies have not been extended to the non-equilibrium FF current noise of a dissipative quantum dot.

A. Functional RG approach

To address this issue, we combine recently developed Functional Renormalization Group (FRG) approach in Refs. 17,31 and the real-time FRG approach in Ref. 63. Within our FRG approaches, as the system moves from the delocalized to the localized phase, we find the smearing of the dips in current noise spectrum for frequencies $\omega \approx \pm V$; more interestingly, we find a peak-to-dip crossover in the AC conductance at $\omega \approx \pm V$.

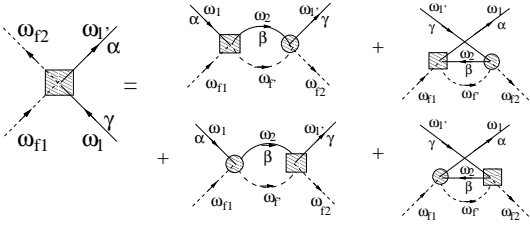


FIG. 12: (Color online) Diagram for renormalization of the current vertex function $L_{\alpha\beta}(\omega_1, \omega'_1)$ (the squares). The solid lines represent conduction electron propagators; the dashed lines denote the pseudo-fermion propagators. Here, the Kondo couplings $g(\omega)$ are denoted by the circles.

These features are detectable in experiments and can serve as alternative signatures (besides conductance) of the QPT in the dissipative resonant level quantum dot.

First, via the above mapping, the current through the dissipative resonant level quantum dot is given by the transverse component of the current $\hat{I}^\perp(t)$ in the effective anisotropic Kondo model as shown in Eq. (10)¹⁶. Following the real-time RG approach in Ref. 63 the Keldysh current operator through the left lead in the effective Kondo model (via a generalization of Eq. (10)) is given by: $\hat{I}_L^\perp(t)$:

$$\hat{I}_L^\perp(t) = \frac{e}{4} \sum_{\kappa} \int dt_1 dt_2 \sum_{\alpha, \beta} \sum dt_1 dt_2 L_{\alpha\beta}^\perp(t_1 - t, t - t_2) \times [s_{\alpha\beta}^+(t_1, t_2) S_f^-(t) + h.c.] \quad (28)$$

with $\alpha, \beta = L, R$, $\vec{S}_f(t) = f^{\kappa\dagger}(t) \vec{\sigma} f^\kappa(t)$, $s_{\alpha\beta}^\pm(t_1, t_2) = c_{\alpha}^{\kappa\dagger}(t_1) \sigma^\pm c_{\beta}^\kappa(t_2)$. Here, $L_{\alpha\beta}(t_1 - t, t - t_2)$ is the left current vertex matrix with bare (initial) matrix elements: $L_{LL}^{0\perp} = L_{RR}^{0\perp} = 0$, $L_{LR}^{0\perp} = -L_{RL}^{0\perp} = ig_{LR}^0 \equiv g_\perp$, $L_{LL}^{0z} = L_{RR}^{0z} \equiv g_z$, $L_{LR}^{0z} = -L_{RL}^{0z} = 0$, and $\kappa = \pm 1$ being the upper and lower Keldysh contour, respectively. The emission component of the non-equilibrium FF noise of a Kondo quantum dot, $S^<(t)$, is given by the current-current correlator:

$$S_{LL}^<(t) \equiv \langle \hat{I}_L^\perp(0) \hat{I}_L^\perp(t) \rangle \quad (29)$$

Similarly, the absorption part of the noise is defined as: $S^>(t) \equiv \langle \hat{I}_L^\perp(t) \hat{I}_L^\perp(0) \rangle$. Note that the current operator $\hat{I}_L^\perp(t)$ is non-local in time under RG; the current vertex function $L_{\alpha\beta}(t_1 - t, t - t_2)$ therefore acquires the double-time structure: it keeps track of not only the times electrons enter (t_1) and leave (t_2) the dot, but also the time t at which the current is measured⁶³. The double-time structure of the current operator automatically satisfies the current conservation: $\hat{I}_L^\perp(t) = -\hat{I}_R^\perp(t)$ (Ref. 63). The frequency-dependent current noise $S(\omega)$ is computed via the second-order renormalized perturbation theory (see diagram in Fig. 11). Note that due to the double-time structure of the current vertex function $L_{\alpha\beta}(t_1, t_2)$, in the Fourier (frequency) space, $L_{\alpha, \beta}(\epsilon + \omega, \epsilon)$ has a two-frequency structure; it depends on the incoming ($\epsilon + \omega$)

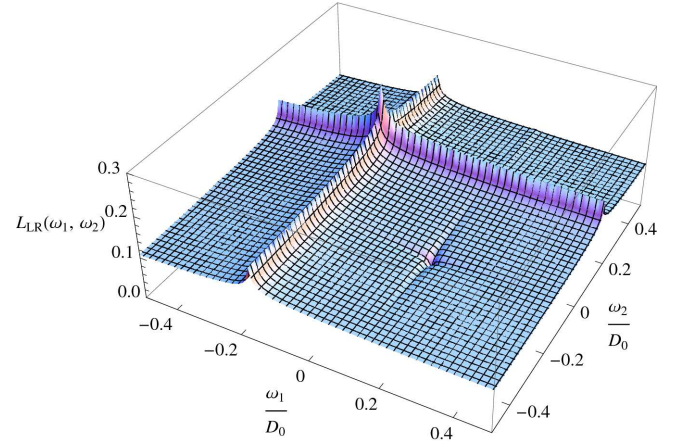


FIG. 13: (Color online) 3D plot for $L_{LR}(\omega_1, \omega_2)$ at zero temperature in the delocalized phase with bare Kondo couplings being $g_\perp^0 = 0.05D_0$, $g_z^0 = 0.05D_0$. The bias voltage is fixed at $V = 0.32D_0$.

and outgoing (ϵ) frequencies of the electron (see Fig. 11). The result reads:

$$S^<(\omega) = \sum_{\alpha, \beta=L,R} -2Re(D_{\alpha\beta}(\omega)^<) \quad (30)$$

where the correlator $D_{\alpha\beta}(\omega)$ is computed by the diagram in Fig. 11:

$$\begin{aligned} D_{\alpha\beta}(\omega)^< &= \int \frac{d\Omega}{2\pi} [\chi_{\alpha\beta}(\Omega, \omega) \chi_f(\Omega)]^<, \\ \chi_{\alpha\beta}(\Omega, \omega) &= \int \frac{d\epsilon}{2\pi} \hat{G}_\alpha(\epsilon) \hat{G}_\beta(\epsilon + \Omega + \omega) \\ &\quad \times L_{\alpha\beta}^\perp(\epsilon + \omega, \epsilon) L_{\beta\alpha}^\perp(\epsilon, \epsilon + \omega), \\ \chi_f(\Omega) &= \int \frac{d\nu}{2\pi} \hat{G}_f(\nu) \hat{G}_f(\nu + \Omega), \end{aligned} \quad (31)$$

where \hat{G} is the Green's function in 2×2 Keldysh space, and its lesser and greater Green's function are related to its retarded, advanced, and Keldysh components by:

$$\begin{aligned} G^< &= (G^K - G^R + G^A)/2 \\ G^> &= (G^K + G^R - G^A)/2 \end{aligned} \quad (32)$$

The lesser ($G^<$) and greater ($G^>$) components of Green's function of the conduction electron in the leads and of the quantum dot (impurity) are given by:

$$\begin{aligned} G_{L/R}^<(\epsilon) &= iA_c(\epsilon) f_{\epsilon - \mu_{L/R}} \\ G_{L/R}^>(\epsilon) &= iA_c(\epsilon) (1 - f_{\epsilon - \mu_{L/R}}) \\ G_{f\sigma}^<(\epsilon) &= 2\pi i \delta(\epsilon) n_{f\sigma}(\epsilon) \\ G_{f\sigma}^>(\epsilon) &= 2\pi i \delta(\epsilon) (n_{f\sigma}(\epsilon) - 1), \end{aligned} \quad (33)$$

where $A_c(\epsilon) = 2\pi N_0 \Theta(D_0 - \epsilon)$ is the density of states of the leads, $n_{f\sigma}(\epsilon) = \langle f_\sigma^\dagger f_\sigma \rangle$ is the occupation number of the pseudofermion which obeys $n_{f\uparrow} + n_{f\downarrow} = 1$, $n_{f\sigma}(\epsilon \rightarrow$

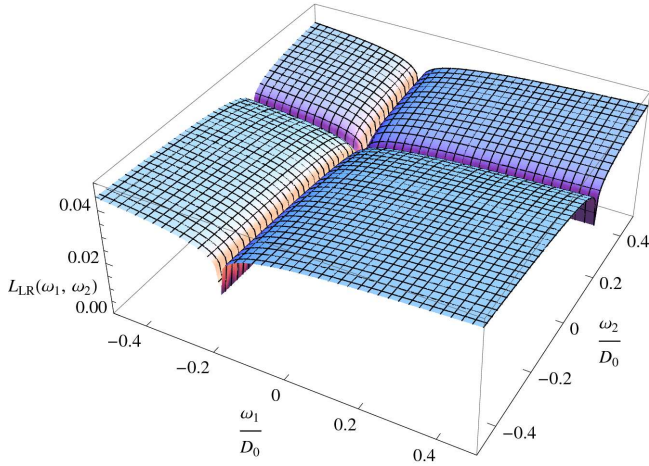


FIG. 14: (Color online) 3D plot for $L_{LR}(\omega_1, \omega_2)$ at zero temperature in the localized phase with bare Kondo couplings being $g_{\perp}^0 = 0.05D_0$, $g_z^0 = -0.1D_0$. The bias voltage is fixed at $V = 0.32D_0$.

$0) = 1/2$ in the delocalized phase and $n_{f\uparrow}(\epsilon \rightarrow 0) \rightarrow 0$, $n_{f\downarrow}(\epsilon \rightarrow 0) \rightarrow 1$ in the localized phase^{16,18}. Here, the pseudofermion occupation number $n_{f\sigma}$ and the occupation number on the dot n_d are related via $\langle n_{f\uparrow} - n_{f\downarrow} \rangle = \langle n_d \rangle - 1/2$ (Refs. 16,17). The renormalized current vertex function $L_{\alpha\beta}^{\perp}(\omega_1, \omega_2)$ and the Kondo couplings $g_{\perp}(\omega)$, $g_z(\omega)$ are obtained from the non-equilibrium Functional RG approaches in Ref. 63 and Refs. 27,31, respectively. Carrying out the calculations, the finite-frequency noise spectrum reads:

$$S^<(\omega) = \sum_{\alpha, \beta=L,R} \frac{3}{8} \int d\epsilon L_{\alpha\beta}^{\perp}(\epsilon + \omega, \epsilon) L_{\beta\alpha}^{\perp}(\epsilon, \epsilon + \omega) \times f_{\epsilon - \mu_{\alpha}}(1 - f_{\epsilon - \mu_{\beta}}), \quad (34)$$

where $f_{\epsilon - \mu_{\alpha}}$ is the Fermi function of the lead $\alpha = L/R$ given by $f_{\epsilon - \mu_{\alpha}} = 1/(1 + e^{(\epsilon - \mu_{\alpha})/k_B T})$. The symmetrized noise spectrum reads:

$$S(\omega) = \frac{1}{2} [S^<(\omega) + S^>(\omega)] \quad (35)$$

with the relation between emission and absorption parts of the noise spectrum in frequency space $S^<(\omega) = S^>(-\omega)$ being used.

The frequency-dependent Kondo couplings $g_{\perp, z}(\omega)$ and current vertex functions $L_{\alpha\beta}^{\perp}(\omega_1, \omega_2)$ are obtained self-consistently within the FRG approaches, which can be divided into two parts. First, the Kondo couplings $g_{\perp, z}(\omega)$ are solved via Eq. (11)^{17,27,31} together with the generalized frequency-dependent dynamical decoherence rate $\Gamma(\omega)$ appearing in $\Theta_{\omega} = \Theta(D - |\omega + i\Gamma(\omega)|)$ in Eq. (11). Here, $\Gamma(\omega)$ is obtained from the imaginary part of the pseudofermion self energy^{17,31,57}:

$$\Gamma(\omega) = \frac{\pi}{4} \int d\epsilon g_{\perp}(\epsilon + \omega) g_{\perp}(\epsilon) [f_{\epsilon}^L - f_{\epsilon + \omega}^R] + g_z(\epsilon + \omega) g_z(\epsilon) [f_{\epsilon}^L - f_{\epsilon + \omega}^L] + (L \rightarrow R). \quad (36)$$

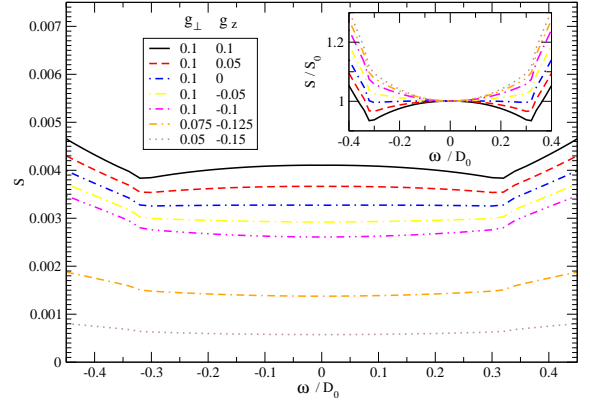


FIG. 15: (Color online) $S(\omega)$ at zero temperature versus ω across the KT transition. The bias voltage is fixed at $V = 0.32D_0$. Inset: $S(\omega)$ at zero temperature versus ω normalized to $S_0 = S(\omega = 0)$.

Note that the zero-frequency decoherence rate $\Gamma(\omega = 0)$ corresponds to the decoherence rate Γ obtained in Eq. (13)²⁷. We have solved the RG equations Eq. (11) subject to Eq. (36) self-consistently⁶⁵.

The solutions for $g_{\perp}(\omega)$, $g_z(\omega)$ and $\Gamma(\omega)$ close to the KT transition are shown in Refs. 16,17 (see also Fig. 2 and Fig. 4). As the system goes from the delocalized to localized phase, the features in $g_{\perp}(\omega)$ at $\omega = \pm V/2$ undergoes a crossover from symmetric two peaks to symmetric two dips, while the symmetric two peaks in $g_z(\omega = \pm V/2)$ still remain peaks. The finite-frequency non-equilibrium decoherence rate $\Gamma(\omega)$ monotonically increases with increasing ω , it shows logarithmic singularities at $|\omega| = V$ in the delocalized phase¹⁷. As the system moves to the localized phase, the overall magnitude of $\Gamma(\omega)$ decreases rapidly and the singular behaviors at $\omega = \pm V$ get smeared out¹⁷.

Next, following Ref. 63, we generalize the RG scaling equation for the general current vertex function $L_{\alpha\beta}(\omega)$ for the anisotropic Kondo model (see diagrams in Fig. 12 and also in Fig. 1 of Ref. 63). The RG scaling equations for the general vertex functions $L_{\alpha\beta}^{\perp, z}(\omega_1, \omega_2)$ can be simplified as:

$$\frac{dL_{\alpha\beta}(\omega_1, \omega_2)}{d \ln D} = \sum_{\gamma=L,R} L_{\alpha\gamma}(\omega_1, \omega_2) \Theta_{\mu_{\gamma}}(\omega_2) g_{\gamma\beta}(\omega_2) + g_{\alpha\gamma}(\omega_1) \Theta_{\mu_{\gamma}}(\omega_1) L_{\gamma\beta}(\omega_1, \omega_2) \quad (37)$$

where we make the following identifications: $g_{LR/RL}(\omega) \rightarrow g_{LR/RL}^{\perp}(\omega) \equiv g_{\perp}(\omega)$, $g_{\alpha\alpha}(\omega) \rightarrow g_{LL/RR}^z(\omega) \equiv g_z(\omega)$. Similarly, $L_{LR/RL}(\omega_1, \omega_2) \rightarrow L_{LR/RL}^{\perp}(\omega_1, \omega_2)$ refers to only the transverse component of the current vertex function $L_{\alpha\beta}(\omega_1, \omega_2)$; while $L_{LL/RR} \rightarrow L_{LL/RR}^z$ refers only to the longitudinal part of $L_{\alpha\alpha}$. Here, the frequency-dependent Kondo couplings $g_{\perp, z\sigma}(\omega)$ in Eq. (37) are obtained from Eq. (11) and Eq. (36). Note that the scaling equations for $L_{\alpha\beta}(\omega_1, \omega_2)$

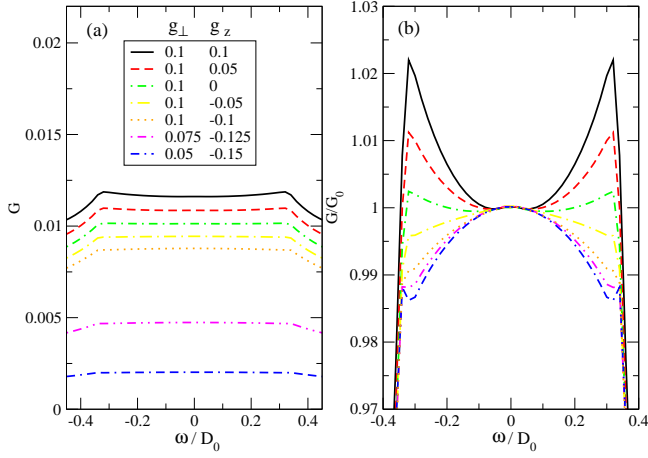


FIG. 16: (Color online) (a) The zero-temperature AC conductance $G_{AC}(\omega)$ defined in Eq. (38) versus ω across the KT transition. (b) $G_{AC}(\omega)$ at zero temperature versus ω normalized to $G_0 \equiv G_{AC}(\omega = 0)$. The bias voltage is fixed at $V = 0.32D_0$.

via Ref. 63 can also be expressed within the RG approach in Ref. 27 via a straightforward generalization by allowing for the two-frequency dependent vertex functions $L_{\alpha\beta}(\omega_1, \omega_2)$ where $\omega_{1(2)}$ refers to the incoming (outgoing) frequency (see Fig. 11 and Fig. 12).

B. Results

We solved the self-consistent RG scaling equations Eq. (37) for the current vertex functions with the help of the solutions for the renormalized Kondo couplings via Eq. (11) and Eq. (36). The typical results at zero temperature are shown in Fig. 13 and Fig. 14; they exhibit the following symmetry: $L_{\alpha\beta}(\omega_1, \omega_2) = -L_{\beta\alpha}(\omega_2, \omega_1)$. Note that since the initial conditions for the current vertex function have the following structures: $L_{\alpha\alpha}^0 = 0$, $L_{LR}^0 \neq 0$, we find $L_{\alpha\alpha}(\omega_1, \omega_2) \ll L_{LR}(\omega_1, \omega_2)$. In the delocalized (Kondo) phase, a sharp peak is developed in $L_{LR}(\omega_1, \omega_2)$ for $(\omega_1, \omega_2) = (V/2, -V/2)$; while as a small dip is formed for $(\omega_1, \omega_2) = (-V/2, V/2)$. Meanwhile, in general $L_{LR}(\omega_1, \omega_2)$ is maximized at $\omega_{1(2)} = \pm V/2$ for fixed $\omega_{2(1)}$. This agrees perfectly with the result in Ref. 63. In the localized phase, however, we find the opposite: $L_{LR}(\omega_1, \omega_2)$ develops a sharp dip at $(\omega_1, \omega_2) = (V/2, -V/2)$; and it is minimized $\omega_{1(2)} = \pm V/2$ for fixed $\omega_{2(1)}$. The peak-dip structure of the current vertex function $L_{\alpha\beta}$ plays a crucial role in determining the noise spectrum both in delocalized and in the localized phases.

Substituting the numerical solutions for $L_{\alpha\beta}(\omega_1, \omega_2)$ and $g_{\alpha\beta}(\omega)$ into Eq. (34), we get the zero-temperature FF noise $S(\omega)$. The results at zero temperature are

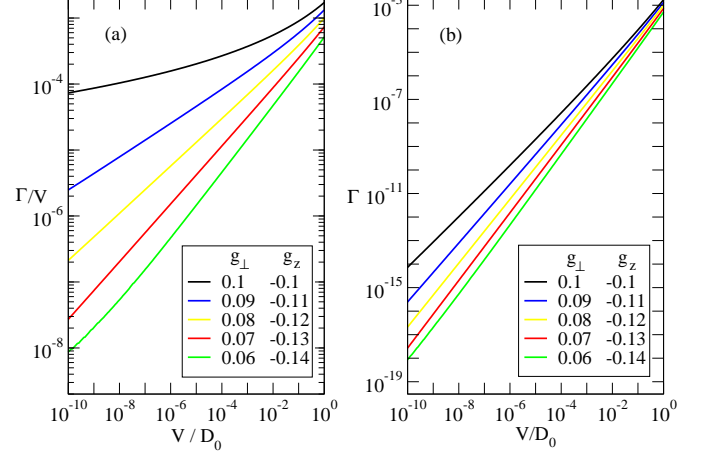


FIG. 17: (a) $\frac{\Gamma}{V}$ and (b) Γ as a function of V/D_0 near the KT transition.

shown in Fig. 15. First, the overall magnitude of $S(\omega)$ decreases rapidly as the system crosses over from the delocalized to the localized phase. This can be understood easily as the current decreases rapidly in the crossover, leading to a rapid decrease in the magnitude of noise. For $|\omega| > V$, $S(\omega)$ in both phases increases monotonically with increasing ω due to the increase of the photon emission at higher energies⁶³. For $|\omega| \leq V$, however, it changes from a peak to a dip centered at $\omega = 0$ as the system crosses over from delocalized to localized phase (see Fig. 15). At $|\omega| = V$, $S(\omega)$ exhibits a dip (minima) in the delocalized phase, a signature of the non-equilibrium Kondo effect; while as the system crosses over to the localized phase the dips are gradually smeared out and they change into a “kink”-like singular point at $\omega = \pm V$, connecting two curves between $\omega < V$ and $\omega > V$.

We furthermore computed the non-equilibrium AC conductance at zero temperature^{63,64}:

$$G_{AC}(\omega) = \frac{S^<(\omega) - S^>(\omega)}{\omega} \quad (38)$$

across the transition. Note that $G(\omega = 0) = dI/dV$ corresponds to the non-equilibrium differential conductance. As shown in Fig. 16 (a), in the delocalized phase the splitted peaks in $G_{AC}(\omega)$ at $\omega = \pm V$ are signatures of the Kondo resonant at finite bias, and are consistent with the dips at seen in the noise spectrum. As the system moves to the localized phase, the overall magnitudes of $G_{AC}(\omega)$ as well as the pronounced splitted Kondo peaks at $\omega = \pm V$ get suppressed; they change into dips deep in the localized phase (see Fig. 16 (b)). In response to this change in the splitted Kondo peaks, the overall shape of $G_{AC}(\omega \rightarrow 0)$ shows a dip-to-hump crossover near $\omega = 0$. Note that the suppression of the Kondo peaks for $G_{AC}(\omega)$ at $\omega = \pm V$ corresponds to the smearing of the dips at $\omega = \pm V$ shown in the noise spectrum $S(\omega)$ (see Fig. 15). The

above evolution in the noise spectrum matches well with the non-equilibrium transport properties studied in Refs. 16,18, and can serve as alternative signatures of the localized-delocalized transition in future experiments.

VI. DISCUSSIONS

We would like to make a few remarks before we conclude. Firstly, the distinct non-equilibrium scaling behavior seen here is in fact closely tied to the non-trivial (non-linear) V dependence of the decoherence rate $\Gamma(V)$ which cuts off the RG flow (see Fig. 17 (a) and (b)). The decoherence rate Γ near the transition clearly plays a very different role as compared to the temperature near the transition. In particular, at $T = 0$ we find that $\Gamma \sim \frac{1}{2}I$ is a highly non-linear function in V , resulting in the observed deviation of the non-equilibrium scaling from that in equilibrium. In fact, we can obtain the analytical form via the approximation in Eq. (18) and Eq. (26). At the KT transition, Γ/V shows a logarithmic decrease as V decreases (see Eqs. (19), (20)); while in the localized phase it exhibits a combined power-law and logarithmic dependence on V (see Eqs. (22), (23), (24), (25), (26)).

By contrast, the equilibrium decoherence rate $\Gamma(V = 0, T)$ shows a clear power-law behavior in the localized phase at low temperatures, $T \rightarrow 0$ (see Eq. (21)):

$$\Gamma(V = 0, T) \propto \left(\frac{T}{T^*}\right)^{1+4c}, \quad (39)$$

which is consistent with the prediction made in Ref. 67 for the electron lifetime in Luttinger liquids.

Meanwhile, at the KT transition and in the localized phase, since $\Gamma \ll V$, the RG flow for $g_{\perp/z}$ are cut off at an energy scale Γ much lower than V , leading to smaller renormalized couplings $g_{\perp/z}$ in magnitude compared to their corresponding equilibrium values $g_{\perp/z}^{(e)}(T = V)$, $|g_{\perp/z}| < |g_{\perp/z}^{(e)}(T = V)|$. This results in smaller conductance than that in equilibrium, $G(V) < G^{eq}(T)$.

Secondly, it is of fundamental importance to study further the possible scaling behaviors in non-equilibrium dynamical quantities near the transition, such as the ω/T scaling in dynamical charge susceptibility at the KT transition and in the localized phase. In particular, the question has been raised on the existence of the concept of “effective temperature” that allows one to extend the fluctuation-dissipation theorem in equilibrium to the non-equilibrium (non-linear) regime⁶⁶. It is also interesting to address the crossover between delocalized phase with $G(V) \propto 1/\ln^2(V/T_K)$ where $\ln T_K \propto 1/(\alpha - \alpha_c)$ to KT point with $G(V) \propto 1/\ln^2(T/\mathcal{D})$ and further to the localized phase with power-law conductance $G(V) \propto V^\beta$.

To date, the full crossover function of the conductance is not known yet. Further study is therefore needed to investigate these issues.

VII. CONCLUSIONS

In summary, we have investigated the non-equilibrium transport at a QPT using a standard nano-model, the dissipative resonant level model. By employing an exact mapping onto the anisotropic Kondo model and by applying a controlled energy-dependent RG and Functional RG approaches to our model system we have calculated the renormalized coupling functions $g_{\perp,z}(\omega)$, the decoherence rate Γ , the current I , differential conductance $G(V, T)$, and the current noise spectrum $S(\omega)$. For $V \rightarrow 0$, the conductance G follows the equilibrium behavior; by increasing V , the frequency-dependence of the couplings begins to play an important role and therefore we systematically find scaling behavior of the non-equilibrium conductance very distinct from that of the equilibrium counterpart. We have also analyzed the finite temperature profile of $G(V, T)$ at the transition as well as in the localized phase and found that the conductance shows different behaviors for $V > T$ and $V < T$; it exhibits V/T scaling behavior for $V \ll T$.

Regarding transport properties of our system near the transition, the role played by the bias voltage is very different from that played by the temperature. The key to these very different behaviors lies in the fact that the non-equilibrium charge (or effective spin) decoherence rate, which serves as a cutoff for the RG flows of the Kondo couplings, is a highly non-linear function of the bias voltage. Further investigations are needed to address the full crossover function in conductance as well as the scaling behaviors of the dynamical quantities near the transition in a search for the existence of the “effective temperature” that allows one to generalize the equilibrium fluctuation-dissipation theorem to the non-equilibrium regime. Furthermore, we provide signatures of the localized-delocalized transition in the finite-frequency current noise spectrum and the AC conductance. Our results have a direct experimental relevance for dissipative two-level systems; moreover, they are applicable for describing non-equilibrium transport of a resonant level coupled to interacting chiral Luttinger liquid generated by fractional quantum Hall edge states via the mappings discussed in Appendix A. Finally, our model system has direct relevance for the recent experiment in a quantum dot coupled to resistive environment as shown in Ref. 43. Our work motivates future experimental as well as theoretical investigations on dissipative quantum phase transitions in nanosystems.

Acknowledgments

We are grateful to D. Goldhaber-Gordon, P. Moca, G. Zarand, and S. Kirchner for stimulating discussions, and to R.T. Chang and K.V.P. Latha for technical support. We acknowledge the generous support from the NSC grant No.98-2112-M-009-010-MY3, No.101-2628-M-009-001-MY3, the MOE-ATU program, the CTS of NCTU, the NCTS of Taiwan, R.O.C. (C.H.C.), the Department of Energy in USA under the contract DE-FG02-08ER46541 (K.L.H.), the German-Israeli Foundation via G 1035-36.14/2009, the DFG via FOR 960 (M.V.,P.W.), GRK 1621 (M.V.), and the Center for Functional Nanostructures CFN (P.W.), the U.S. Department of Energy, Office of Basic Energy Sciences, Division of Materials Sciences and Engineering under Award de-sc0002765 (G.F.). C.H.C. has benefitted from the visiting programs of KITP, ICTP, and MPI-PKS. K.L.H. acknowledges KITP for hospitality. G.F. thanks NCTS, NCTU of Taiwan R.O.C. for hospitality during the visit.

Appendix A: Useful mappings

In this Appendix, we provide detailed derivations on various mappings mentioned in Sec. II. Via bosonization and refermionization techniques, the three mappings described below will follow one from the other, but there are a few technical details that will change.

1. Mapping a dissipative resonant level model onto anisotropic Kondo model

We describe in details on the mapping of dissipative resonant level model in Eq. (2) onto anisotropic Kondo model in Eq. (4). Our goal is to connect the parameters of these two equations in the main text.

We first start from Eq. (2):

$$H = \sum_{k,i=1,2} (\epsilon(k) - \mu_i) c_{ki}^\dagger c_{ki} + t_i c_{ki}^\dagger d + h.c. \quad (\text{A1})$$

$$+ \sum_r \lambda_r (d^\dagger d - 1/2) (b_r + b_r^\dagger) + \sum_r \omega_r b_r^\dagger b_r,$$

where t_i is the (real-valued) hopping amplitude between the lead i and the quantum dot, c_{ki} and d are electron operators for the (Fermi-liquid type) leads and the quantum dot, respectively. $\mu_i = \pm V/2$ is the chemical potential applied on the lead i (V denotes the bias voltage), while the dot level is at zero chemical potential. Here, b_r are the boson operators of the dissipative bath with an Ohmic type spectral density. It proves to be more convenient to re-express the dissipative boson fields b_r and b_r^\dagger in terms of the canonical fields $\hat{\phi}_0(x, t)$ and $\hat{\Pi}_0(x, t)$

as:^{7,55}:

$$\hat{\phi}_0(x, t) = \int_{-\infty}^{\infty} \frac{dp}{2\pi\sqrt{2|p|}} [b_p e^{ipx} + b_p^\dagger e^{ipx}] e^{-a|p|/2}$$

$$\hat{\Pi}_0(x, t) = \partial_t \hat{\phi}_0(x, t) \quad (\text{A2})$$

where $\omega_r = v_b p_r$ with v_b being the phonon velocity, and the boson fields $\hat{\phi}_0(x, t)$ and $\hat{\Pi}_0(x, t)$ satisfies the commutation relation: $[\hat{\phi}_0(x, t), \hat{\Pi}_0(x', t)] = i\delta(x - x')$. The dissipative boson bath can therefore be re-expressed as:

$$H_{diss} = \sum_r \omega_r b_r^\dagger b_r = \int \frac{dp}{2\pi} |p| b_p^\dagger b_p$$

$$= \frac{1}{2} \int dx [(\partial_x \hat{\phi}_0)^2(x, t) + \hat{\Pi}_0^2(x, t)]. \quad (\text{A3})$$

Here, the velocity of the boson field $\hat{\phi}_0$ is set to be 1.

We start the mapping by bosonizing the fermionic operators in the leads:

$$c_\alpha(0) = \frac{1}{\sqrt{2\pi a}} F_\alpha e^{i\varphi_\alpha(0)}, \quad (\text{A4})$$

where we have introduced the (standard) Klein factors F_α ensuring anti-commutation relations and a is a short-distance cutoff (lattice spacing). The fermionic baths of conduction electrons can be re-written as:

$$H_{leads} = \sum_{k,i=1,2} (\epsilon(k) - \mu_i) c_{ki}^\dagger c_{ki}$$

$$= \frac{1}{2} \int dx \sum_{\alpha=1,2} [(\partial_x \varphi_\alpha)^2(x, t) + \Pi_\alpha^2(x, t)] \quad (\text{A5})$$

where the Fermi velocity of the electrons is set to be 1.

The level on the quantum dot can be mapped onto a pseudo-spin: $d = F_d S^-$ and $S^z = d^\dagger d - 1/2$; $\alpha = 1, 2$ represent the two leads. The coupling between the dot and the dissipation bath (λ_i term) can be absorbed in the tunneling part of the Hamiltonian through the unitary transformation U_B ⁷:

$$U_B = e^{i\sqrt{\frac{1}{K_b}} S_z \hat{\phi}_0} \quad (\text{A6})$$

$$\hat{H}_t = U_B^\dagger H_t U_B$$

$$= \sum_{\alpha=1,2} t_\alpha F_\alpha^\dagger F_\alpha e^{i\sqrt{\frac{1}{K_b}} \hat{\phi}_0} e^{i\varphi_\alpha(0)} S^- + H.c.$$

with $K_b \equiv \frac{1}{\alpha}$. Here, α refers to the strength of the coupling between the resonant level and the dissipative boson bath, and we set $2\pi a = 1$ for simplicity.

We can simplify our variables even further by combining the above fields describing the leads and the noise: $\tilde{\varphi}_{s,\alpha} = \sqrt{K}(\varphi_\alpha + \sqrt{\frac{1}{K_b}} \hat{\phi}_0)$, $\tilde{\varphi}_{a,\alpha} = \sqrt{K}(\sqrt{\frac{1}{K_b}} \varphi_\alpha - \hat{\phi}_0)$, where $\frac{1}{K} = \frac{1}{K_b} + 1 = \alpha + 1 \equiv \frac{1}{\alpha^*}$. Note that here K may be interpreted as the effective Luttinger liquid parameter as the effect of Ohmic dissipation on the quantum dot

plays a similar role as interactions in the Luttinger liquid leads coupled to the dot with the identification $K = \frac{1}{1+\alpha}$. The combined bosonic and fermionic bath \tilde{H}_{bath} can be re-expressed in terms of these new boson fields:

$$\begin{aligned}\tilde{H}_{bath} &\equiv H_{leads} + H_{diss} \\ &= \frac{1}{2} \int dx \sum_{\alpha=1,2} [(\partial_x \varphi_\alpha)^2(x,t) + \Pi_\alpha^2(x,t)] \\ &+ \frac{1}{2} \int dx [(\partial_x \hat{\phi}_0)^2(x,t) + \hat{\Pi}_0^2(x,t)] \\ &= \frac{1}{2} \int dx \sum_{\alpha=1,2} [(\partial_x \tilde{\phi}_{s,\alpha})^2(x,t) + \hat{\Pi}_{s,\alpha}^2(x,t) \\ &+ (\partial_x \tilde{\phi}_{a,\alpha})^2(x,t) + \hat{\Pi}_{a,\alpha}^2(x,t)],\end{aligned}\quad (A7)$$

where $\Pi_{s(a),\alpha}$ fields are canonically conjugate to the fields $\tilde{\phi}_{s(a),\alpha}$. Note that as we shall see below only the fields from symmetric combinations $\tilde{\phi}_{s,\alpha}$ and $\Pi_{s,\alpha}$ couple to the tunneling and chemical potential terms, the antisymmetric combinations $\tilde{\phi}_{a,\alpha}$ and $\Pi_{a,\alpha}$ are de-coupled from the rest of the Hamiltonian.

The tunneling and chemical potential parts of the Hamiltonian now become:

$$\tilde{H}_t = U_B^\dagger H_t U_B = \sum_{\alpha=1,2} t_\alpha F_\alpha^\dagger F_d e^{i\frac{\tilde{\phi}_{s,\alpha}}{\sqrt{K}}} S^- + H.c. \quad (A8)$$

$$\tilde{H}_\mu = U_B^\dagger H_\mu U_B = -\frac{V}{2} \sqrt{\frac{1}{K}} (\partial_x \tilde{\phi}_{s,1} - \partial_x \tilde{\phi}_{s,2})$$

Close to $\alpha^* = 1/2$ (transition), we can map our model onto the 2-channel anisotropic Kondo model. After applying the two unitary transformations $U_1 = e^{i(\frac{\tilde{\phi}_{s,1}}{\sqrt{K}} - \sqrt{2}\tilde{\phi}_{s,1})S_z}$ and $U_2 = e^{i(\frac{\tilde{\phi}_{s,2}}{\sqrt{K}} - \sqrt{2}\tilde{\phi}_{s,2})S_z}$, we obtain:

$$\begin{aligned}\tilde{H}_t'' &= U_2^\dagger U_1^\dagger \tilde{H}_t U_1 U_2 \\ &= [t_1 F_1^\dagger F_d e^{i(\sqrt{2} - \frac{1}{\sqrt{K}})\tilde{\phi}_{s,2}} e^{i\sqrt{2}\tilde{\phi}_{s,1}} \\ &+ t_2 F_2^\dagger F_d e^{i(\sqrt{2} - \frac{1}{\sqrt{K}})\tilde{\phi}_{s,1}} e^{i\sqrt{2}\tilde{\phi}_{s,2}}] S^- + H.c. \\ &- (\sqrt{2} - \frac{1}{\sqrt{K}}) (\partial_x \tilde{\phi}_{s,1} + \partial_x \tilde{\phi}_{s,2}) S_z\end{aligned}\quad (A9)$$

Note that there are additional phase factors $e^{i(\sqrt{2} - \frac{1}{\sqrt{K}})\tilde{\phi}_{s,\alpha}}$ in the hopping terms. Since we are interested in the physics close to the localized-delocalized transition, i.e., $K = \alpha^* \rightarrow 1/2$, we may drop these phase factors in the following analysis. The chemical potential term after the above two transformations now becomes

$$\begin{aligned}\tilde{H}_\mu'' &= U_2^\dagger U_1^\dagger \tilde{H}_\mu U_1 U_2 \\ &= -\frac{V}{2} \sqrt{\frac{1}{2K}} [\partial_x (\sqrt{2}\tilde{\phi}_{s,1}) - \partial_x (\sqrt{2}\tilde{\phi}_{s,2})]\end{aligned}\quad (A10)$$

Note that since the hopping \tilde{H}_t'' and chemical potential \tilde{H}_μ'' terms involve only $\tilde{\phi}_{s,\alpha}$ fields, $\tilde{\phi}_{a,\alpha}$ fields are decoupled from the Hamiltonian.

Now, we can refermionize the bosons and map our transformed Hamiltonian

$$\tilde{H}_{RLM} \equiv \tilde{H}_{bath} + \tilde{H}_t'' + \tilde{H}_\mu'' \quad (A11)$$

onto the anisotropic Kondo model in Eq. (4) via the following identifications:

$$\begin{aligned}-\sqrt{2}\tilde{\phi}_{s,1} &= \Phi_L^\dagger - \Phi_R^\dagger \\ -\sqrt{2}\tilde{\phi}_{s,2} &= \Phi_R^\dagger - \Phi_L^\dagger \\ c_{L/R}^\sigma(0) &= F_{L/R}^\sigma e^{i\Phi_{L/R}^\sigma}\end{aligned}\quad (A12)$$

where $F_{L/R}^\sigma$ is the Klein factor for the effective lead L and R , respectively.

To see the equivalence between these two models, we bosonize Eq. (4) and compare it with Eq. (A11):

$$\begin{aligned}H_K &= H_{leads} + H_{J_\perp} + H_{J_z}, \\ H_{leads} &= \sum_{k,\gamma=L,R,\sigma=\uparrow,\downarrow} [\epsilon_k - \mu_\gamma] c_{k\gamma\sigma}^\dagger c_{k\gamma\sigma} \\ &= \frac{1}{2} \int dx \sum_{\alpha=L,R} [(\partial_x \Phi_\alpha)^2(x,t) + \Pi_\alpha^2(x,t)] \\ &- \frac{V}{2} \sqrt{\frac{1}{2K}} \sum_{\sigma=\uparrow,\downarrow} [\partial_x \Phi_L^\sigma - \partial_x \Phi_R^\sigma], \\ H_{J_\perp} &= J_\perp^{(1)} s_{LR}^+ S^- + J_\perp^{(2)} s_{RL}^+ S^- + h.c. \\ &= J_\perp^{(1)} F_L^\dagger F_R^\dagger F_R^\dagger e^{i\Phi_L^\dagger - i\Phi_R^\dagger} + J_\perp^{(2)} F_R^\dagger F_L^\dagger e^{i\Phi_R^\dagger - i\Phi_L^\dagger}, \\ H_{J_z} &= \sum_{\gamma=L,R} J_z s_{\gamma\gamma}^z S^z \\ &= -J_z \sum_{\alpha=L,R} [\partial_x \Phi_\alpha^\dagger - \partial_x \Phi_\alpha^\dagger]\end{aligned}\quad (A13)$$

With the proper redefinitions of the Klein factors: $F_1^\dagger F_d \equiv F_L^\dagger F_R^\dagger$, $F_1^\dagger F_d \equiv F_R^\dagger F_L^\dagger$, and the identifications: $d = S^-$, $d^\dagger = S^+$, $d^\dagger d - 1/2 = S_z$, $J_\perp^{(\alpha)} = t_\alpha$, $J_z = 1 - \frac{1}{\sqrt{2K}}$, we finally establish the equivalence between a Kondo model with the effective left (L) and right lead (R) in Eq. (4) and a dissipative resonant level model in Eq. (A11).

2. Mapping a dissipative resonant level model onto a resonant level coupled to FQHE

We provide details here on the mapping of a dissipative resonant level model Eq. (2) onto a resonant level coupled to Fractional Quantum Hall Edge states (FQHE) as shown in Eq. (6).

We start from the Hamiltonian Eq. (6) describing a resonant level coupled to two FQHE states:

$$H_{FQHE} = H_{chiral} + H_t + H_\mu, \quad (A14)$$

where the lead term H_{chiral} describes two chiral Luttinger liquid leads with lead index $\alpha = 1, 2$, H_t denotes the tunneling term and the bias voltage term H_μ is given respectively by:

$$\begin{aligned} H_{chiral} &= \frac{1}{2} \int_{-\infty}^{+\infty} \sum_{\alpha=1,2} \left(\frac{d\varphi_\alpha}{dx} \right)^2 dx, \\ H_t &= t_1 e^{i\varphi_1/\sqrt{K}} d + t_2 e^{i\varphi_2/\sqrt{K}} d + h.c., \\ H_\mu &= -\frac{V}{2} \frac{1}{\sqrt{K}} (\partial\varphi_1 - \partial\varphi_2), \end{aligned} \quad (\text{A15})$$

where the boson field $\varphi_{\alpha=1,2}$ denotes the chiral Luttinger liquid in lead α , the tunneling between lead and the resonant level is given by t_α , V is the bias voltage, and K refers to the Luttinger parameter.

Via similar Unitary transformations mentioned above, $U_1 = e^{i(\frac{\varphi_1}{\sqrt{K}} - \sqrt{2}\varphi_1)S_z}$ and $U_2 = e^{i(\frac{\varphi_2}{\sqrt{K}} - \sqrt{2}\varphi_2)S_z}$, Eq. (6) now becomes:

$$\tilde{H}_{FQHE} = U_2^\dagger U_1^\dagger H_{FQHE} U_1 U_2 = H_{chiral} + \tilde{H}_t + \tilde{H}_\mu, \quad (\text{A16})$$

where the tunneling term H_t in Eq. (A15) becomes (assuming $t_1 = t_2 = t$):

$$\begin{aligned} \tilde{H}_t &= t [e^{i(\sqrt{2} - \frac{1}{\sqrt{K}})\varphi_2} e^{i\sqrt{2}\varphi_1} \\ &+ e^{i(\sqrt{2} - \frac{1}{\sqrt{K}})\varphi_1} e^{i\sqrt{2}\varphi_2}] S^- + h.c. \\ &- (1 - \sqrt{\frac{1}{2K}}) (\partial\sqrt{2}\varphi_1 + \partial\sqrt{2}\varphi_2) S_z, \end{aligned} \quad (\text{A17})$$

and the chemical potential term in Eq. (A15) becomes

$$\tilde{H}_\mu = -\frac{V}{2} \sqrt{\frac{1}{2K}} [\partial_x(\sqrt{2}\varphi_1) - \partial_x(\sqrt{2}\varphi_2)]. \quad (\text{A18})$$

The equivalence between a resonant level coupled to FQHE Eq. (6) and a dissipative resonant level model Eq. (2) is established by comparing the transformed Hamiltonian \tilde{H}_{FQHE} in Eq. (A16) for the former model and \tilde{H}_{RLM} (see Eq. (A7), (A10), and (A11)) for the latter one.

3. Mapping a dissipative resonant level onto a dissipative resonant level coupled to chiral Luttinger liquid leads

Below we provide details on the mapping of a large dissipative resonant level onto a large resonant level (spinless quantum dot) with Ohmic dissipation coupled to two chiral Luttinger liquid leads. The mapping is easily extended to the latter case with a small (single-level) resonant level.

First, we take the same dissipative boson environment as shown in Eq. (A3). Via standard bosonization (see Eq. (5)), the Luttinger leads and the chemical potential term take the same bosonized form as Eq. (A5) and

Eq. (7), respectively. The remaining parts of the Hamiltonian are modified as follows:

$$\begin{aligned} H_{dot} &= H_d + H_t + H_{db}, \\ H_d &= \sum_k \epsilon_{d_k} d_k^\dagger d_k, \\ H_t &= \sum_{k,k',\alpha=1,2} t_\alpha c_{k,\alpha}^\dagger d_{k'} S^- + h.c., \\ H_{db} &= \sum_{r,k'} \lambda_r (d_{k'}^\dagger d_{k'} - 1/2) (b_r + b_r^\dagger), \end{aligned} \quad (\text{A19})$$

where ϵ_{d_k} refers to the energy spectrum of the many-level dot, the electron destruction operator on the dot $d(0)$ is defined as: $d(0) = \sum_k d_k$, and spin-flip operator S^\pm represents for the hoping of charge between lead and the dot⁷. We then bosonize the electron operators in the leads (see Eq. (5)) and on the dot: $d(0) = \frac{1}{\sqrt{2\pi a}} F_d e^{i\phi_d}$. Via the unitary transformation U_B defined in Eq. A7, we arrive at:

$$\begin{aligned} \tilde{H}_t &= U_B^\dagger H_t U_B \\ &= \sum_{\alpha=1,2} t_\alpha F_\alpha^\dagger F_d e^{i\sqrt{\frac{1}{K_b}}\hat{\phi}_0} e^{i(\frac{\varphi_\alpha(0)}{\sqrt{K}} - \phi_d)} S^- + H.c. \end{aligned} \quad (\text{A20})$$

To further simplify the hoping term, we define new boson fields $\phi_{s(a),\alpha}$ via linear combinations of the fields ($\varphi_\alpha(0)$ and ϕ_d):

$$\begin{aligned} \phi_{a,\alpha} &= \sqrt{K'} \left(\frac{\varphi_\alpha(0)}{\sqrt{K}} - \phi_d \right), \\ \phi_{s,\alpha} &= \sqrt{K'} \left(\frac{\varphi_\alpha(0)}{\sqrt{K}} + \phi_d \right) \end{aligned} \quad (\text{A21})$$

with $\frac{1}{K'} = \frac{1}{K} + 1$. The combined fermionic baths of the leads and the dot are given by:

$$\begin{aligned} H_f &\equiv H_{leads} + H_d \\ &= \frac{1}{2} \int dx \sum_{\alpha=1,2} [(\partial_x \phi_{s,\alpha})^2(x,t) + \tilde{\Pi}_{s,\alpha}^2(x,t) \\ &+ (\partial_x \phi_{a,\alpha})^2(x,t) + \tilde{\Pi}_{a,\alpha}^2(x,t)], \end{aligned} \quad (\text{A22})$$

where $\tilde{\Pi}_{s(a),\alpha}$ are canonically conjugate boson fields to $\phi_{s(a),\alpha}$ fields. In terms of the new fields $\phi_{s(a),\alpha}$, the hoping and chemical potential terms now become:

$$\begin{aligned} \tilde{H}_t &= \sum_{\alpha=1,2} t_\alpha F_\alpha^\dagger F_d e^{i\sqrt{\frac{1}{K_b}}\hat{\phi}_0} e^{i\frac{\phi_{a,\alpha}}{\sqrt{K'}}} S^- + H.c., \\ H_\mu &\rightarrow \tilde{H}_\mu \\ &= -\frac{V}{2} \sqrt{\frac{K}{K'}} [\partial_x(\phi_{a,1}) - \partial_x(\phi_{a,2})]. \end{aligned} \quad (\text{A23})$$

We may furthermore combine the boson fields from the leads $\phi_{a,\alpha}$ and from the dissipative bath $\hat{\phi}_0$ via the fol-

lowing definitions:

$$\begin{aligned}\tilde{\phi}_{s,\alpha} &= \sqrt{\tilde{K}}\left(\frac{\phi_{a,\alpha}}{K'} + \sqrt{\frac{1}{K_b}}\hat{\phi}_0\right), \\ \tilde{\phi}_{a,\alpha} &= \sqrt{\tilde{K}}\left(\frac{\phi_{a,\alpha}}{K'} - \sqrt{\frac{1}{K_b}}\hat{\phi}_0\right),\end{aligned}\quad (\text{A24})$$

where $\frac{1}{\tilde{K}} = \frac{1}{K'} + \frac{1}{K_b}$. Upon applying the unitary transformation, the combined fermionic and bosonic baths terms become:

$$\begin{aligned}H_f &= \frac{1}{2} \int dx \sum_{\alpha=1,2} [(\partial_x \tilde{\phi}_{s,\alpha})^2(x,t) + \bar{\Pi}_{s,\alpha}^2(x,t) \\ &\quad + (\partial_x \tilde{\phi}_{a,\alpha})^2(x,t) + \bar{\Pi}_{a,\alpha}^2(x,t)],\end{aligned}\quad (\text{A25})$$

where $\bar{\Pi}_{s(a),\alpha}$ are canonically conjugate boson fields to $\tilde{\phi}_{s(a),\alpha}$ fields.

Meanwhile, the corresponding hopping and chemical potential terms become:

$$\begin{aligned}\tilde{H}_t &= \sum_{\alpha=1,2} t_\alpha F_\alpha^\dagger F_\alpha e^{i\frac{\tilde{\phi}_{s,\alpha}}{\sqrt{\tilde{K}}}} S^- + H.c., \\ H_\mu &\rightarrow \tilde{H}_\mu \\ &= -\frac{V}{2} \sqrt{\frac{K'}{\tilde{K}}} [\partial_x(\tilde{\phi}_{s,1}) - \partial_x(\tilde{\phi}_{s,2})].\end{aligned}\quad (\text{A27})$$

Via the similar Unitary transformation mentioned above, $U_1 = e^{i(\frac{\tilde{\phi}_1}{\sqrt{\tilde{K}}} - \sqrt{2}\varphi_1)S_z}$ and $U_2 = e^{i(\frac{\tilde{\phi}_2}{\sqrt{\tilde{K}}} - \sqrt{2}\tilde{\phi}_{s,2})S_z}$, the tunneling term becomes (assuming $t_1 = t_2 = t$):

$$\begin{aligned}H_t &= t[e^{i(\sqrt{2} - \frac{1}{\sqrt{\tilde{K}}})\tilde{\phi}_{s,2}} e^{i\sqrt{2}\tilde{\phi}_{s,1}} \\ &\quad + e^{i(\sqrt{2} - \frac{1}{\sqrt{\tilde{K}}})\varphi_1} e^{i\sqrt{2}\tilde{\phi}_{s,2}}] S^- + h.c. \\ &\quad - (1 - \sqrt{\frac{1}{2\tilde{K}}})(\partial\sqrt{2}\tilde{\phi}_{s,1} + \partial\sqrt{2}\tilde{\phi}_{s,2})S_z.\end{aligned}\quad (\text{A28})$$

The chemical potential term therefore becomes

$$\begin{aligned}H_\mu &\rightarrow \tilde{H}_\mu \\ &= -\frac{V}{2} \sqrt{\frac{K'}{\tilde{K}}} [\partial_x(\sqrt{2}\tilde{\phi}_{s,1}) - \partial_x(\sqrt{2}\tilde{\phi}_{s,2})].\end{aligned}\quad (\text{A29})$$

We may now follow the same refermionization procedure as shown in Eq. (A13) to map our Hamiltonian onto the anisotropic Kondo model in the same form as Eq. (4) with the following identifications:

$$\begin{aligned}J_\perp^{(1),(2)} &\propto t_\alpha e^{i(\sqrt{2} - \frac{1}{\tilde{K}})\tilde{\phi}_{s,2,1}}, \\ J_z &\propto 1 - \frac{1}{2\tilde{K}}, \\ \mu &\rightarrow \tilde{\mu} = \frac{V}{2} \sqrt{\frac{K'}{\tilde{K}}}.\end{aligned}\quad (\text{A30})$$

The above mapping can easily be generalized to a small quantum dot with single resonant level with \tilde{K} given by Eq. (9) where the contribution from the many-level big dot is absent here.

Appendix B: Average currents.

In this Appendix, we prove that the average currents in the original model \hat{I}_{ori} is equivalent to that in the effective Kondo model \hat{I}_{Kondo} . The current operators in both models are given by:

$$\begin{aligned}\hat{I}_{ori} &= d/dt(N_1 - N_2) \\ &= it_1 \sum_k (c_{k1}^\dagger d - d^\dagger c_{k1}) - (1 \rightarrow 2)\end{aligned}\quad (\text{B1})$$

$$\begin{aligned}\hat{I}_{Kondo} &= d/dt(N_L - N_R) \\ &= iJ_\perp^{(1)}(s_{LR}^- S^+ - s_{RL}^+ S^-) - (1 \rightarrow 2, L \rightarrow R)\end{aligned}\quad (\text{B2})$$

On the other hand, from the bosonized forms of the two models, (at the transition) we have:

$$\begin{aligned}\langle \hat{I}_{ori} \rangle &= \langle d/dt(N_1 - N_2) \rangle \\ &= \int dx \langle \frac{d}{dt} [\partial_x \varphi_1 - \partial_x \varphi_2] \rangle \\ &= \int dx \sqrt{\frac{1}{2K}} \langle \frac{d}{dt} [\partial_x(\sqrt{2}\tilde{\phi}_{s,1}) - \partial_x(\sqrt{2}\tilde{\phi}_{s,2})] \rangle\end{aligned}\quad (\text{B3})$$

$$\begin{aligned}\langle \hat{I}_{Kondo} \rangle &= \langle d/dt(N_L - N_R) \rangle \\ &= \int dx \langle d/dt \sum_{\sigma=\uparrow,\downarrow} [\partial_x \Phi_L^\sigma - \partial_x \Phi_R^\sigma] \rangle \\ &= \int dx \langle d/dt [\partial_x(\sqrt{2}\tilde{\phi}_{s,1}) - \partial_x(\sqrt{2}\tilde{\phi}_{s,2})] \rangle\end{aligned}\quad (\text{B4})$$

Therefore, we have

$$\langle \hat{I}_{ori} \rangle = \frac{1}{\sqrt{2K}} \langle \hat{I}_{Kondo} \rangle\quad (\text{B5})$$

(or $\langle \hat{I}_{ori} \rangle = \frac{1}{\sqrt{2\alpha^*}} \langle \hat{I}_{Kondo} \rangle$). The above relation obtained so far from the mapping is exact at finite bias voltages. In the limit of our interest $K = \alpha^* \rightarrow 1/2$, $\langle \hat{I}_{ori} \rangle = \langle \hat{I}_{Kondo} \rangle$.

We can also prove this equivalence through Keldysh perturbation theory. We now would like to prove that

$$\langle \hat{I}_{Kondo} \rangle_K = \langle \hat{I}_{ori} \rangle_{ori}\quad (\text{B6})$$

where

$$\begin{aligned}\langle I_{Kondo}(t) \rangle_K &= \frac{1}{Z_K} \\ &\quad \times Tr[e^{-\beta H_K} T_c(S_c^K(-\infty, \infty) I_{Kondo}(t))] \\ Z_K &= Tr[e^{-\beta H_K} T_c(S_c^K(-\infty, \infty))] \\ S_c^K(-\infty, \infty) &= e^{-i \int_c dt' H_K^{eq}(t')}\end{aligned}\quad (\text{B8})$$

and

$$\begin{aligned}\langle \hat{I}_{ori}(t) \rangle_{ori} &= \frac{1}{Z_{ori}} Tr[e^{-\beta H} T_c(S_c^{ori}(-\infty, \infty) \hat{I}_{ori}(t))] \\ Z_{ori} &= Tr[e^{-\beta H} T_c(S_c^{ori}(-\infty, \infty))] \\ S_c^{ori}(-\infty, \infty) &= e^{-i \int_c dt' H^{eq}(t')}\end{aligned}\quad (\text{B9})$$

Here $H_K^{eq}(H^{eq})$ is the Kondo (original) Hamiltonian in equilibrium ($\mu = 0$), $T_c(\dots)$ orders the operators along the Keldysh contour c .

1. We first show that $Z_K = Z_{ori}$ (the two partition functions from the original and the effective Kondo models are equivalent) where

$$\begin{aligned}Z_{ori} &= Tr[e^{-\beta H} T_c(S_c^{ori}(-\infty, \infty))] \quad (\text{B10}) \\ S_c^{ori}(-\infty, \infty) &= e^{-i \int_c dt' H^{eq}(t')}\end{aligned}$$

To prove this, we first note that the original and the effective Kondo models are related by the above-mentioned unitary transformations: $H_K = U^\dagger H U$ with $U = U_2 U_1 U_B$. The similar relation holds for the current operators: $\hat{I}_{Kondo} = U^\dagger \hat{I}_{ori} U$. Using the following identities:

$$\begin{aligned}e^{-\int_0^\beta d\tau U^\dagger(\tau) H(\tau) U(\tau)} &\quad (\text{B11}) \\ &= \sum_{n=0}^{\infty} \frac{(-1)^n}{n!} \left[\int_0^\beta d\tau (U^\dagger(\tau) H(\tau) U(\tau))^n \right]\end{aligned}$$

where

$$\begin{aligned}Tr[\hat{A}(\tau) \hat{B}(\tau) \hat{C}(\tau)] &= Tr[\hat{C}(\tau) \hat{A}(\tau) \hat{B}(\tau)] \\ &= Tr[\hat{B}(\tau) \hat{C}(\tau) \hat{A}(\tau)] = \dots \quad (\text{B12})\end{aligned}$$

with $\tau = it$ the imaginary time and $\hat{A}, \hat{B}, \hat{C}$ being any quantum mechanical operators we can then show that $Z_K = Z_{ori}$. In other words, when the Hamiltonian is under above unitary transformations, the trace in the partition function remains unchanged.

2. In the similar way, we can prove that:

$$\begin{aligned}Tr[e^{-\beta H_K} T_c(S_c^K(-\infty, \infty) I_{Kondo}(t))] &\quad (\text{B13}) \\ &= Tr[e^{-\beta H} T_c(S_c^{ori}(-\infty, \infty) I_{ori}(t))]\end{aligned}$$

where we have used Eq. (B11) and $\hat{I}_{Kondo} = U^\dagger \hat{I}_{ori} U$.

From 1. and 2. mentioned above, we conclude that $\langle \hat{I}_{Kondo}(t) \rangle_K = \langle \hat{I}_{ori}(t) \rangle_{ori}$ holds for all orders in Keldysh perturbation theory.

Appendix C: Non-equilibrium current for $t_1 \neq t_2$.

In this Appendix, we derive the general expression for the average current for $t_1 \neq t_2$. From Eq. (B3), the

average current in the Kondo model is given by:

$$\langle \hat{I} \rangle = \int_{-\infty}^{\infty} \sum_k J_\perp^{(1)} (G_{k,d}^<(\omega) - G_{k,d}^>(\omega)) - (1 \rightarrow 2, L \rightarrow R) \quad (\text{C1})$$

where $G_{k,d}^<(t) = i \langle s_{LR}^- S_d(t) \rangle$. Following Ref.58, the Dyson's equation for $G_{k,d}^<(\omega)$ is given by:

$$\begin{aligned}G_{k,d}^<(\omega) &= J_\perp^{(1)} [\chi_{LR}^{+-t}(\omega) \chi_d^{+<}(\omega) \\ &\quad - \chi_{LR}^{+-<}(\omega) \chi_d^{+t}(\omega)] - (1 \rightarrow 2, L \rightarrow R)\end{aligned}\quad (\text{C2})$$

where $\chi_{LR}^{+-<}(t) = \langle s_{LR}^- s_{LR}^+(t) \rangle$, $\chi_{LR}^{+->}(t) = \langle s_{LR}^-(t) s_{LR}^+ \rangle$, $\chi_d^{+<} = \langle S_d^- S_d^+(t) \rangle$, $\chi_{LR}^{+-t}(\omega)$, and χ_d^{+t} are time-order and anti-timeordered Green's functions, respectively. The following relations hold among these correlation functions:

$$\begin{aligned}\chi^<(\omega) + \chi^>(\omega) &= \chi^t(\omega) + \chi^{\tilde{t}}(\omega) \\ \chi^>(\omega) - \chi^<(\omega) &= \chi^R(\omega) - \chi^A(\omega)\end{aligned}\quad (\text{C3})$$

where $\chi^{R/A}(\omega)$ is the retarded (advanced) Green's function, respectively. Straightforward calculation gives:

$$\begin{aligned}\chi_{LR}^{+-<}(\omega) &= 2\pi f_{\omega-\mu_L} (1 - f_{\omega-\mu_R}) \delta(\omega - \epsilon(k)) \\ \chi_{LR}^{+->}(\omega) &= -2\pi f_{\omega-\mu_R} (1 - f_{\omega-\mu_L}) \delta(\omega - \epsilon(k))\end{aligned}\quad (\text{C4})$$

The average current reads

$$\begin{aligned}\langle \hat{I} \rangle &= \int_{-\infty}^{\infty} [f_{\omega-\mu_L} (1 - f_{\omega-\mu_R}) \tilde{\Gamma}_1 \\ &\quad - f_{\omega-\mu_R} (1 - f_{\omega-\mu_L}) \tilde{\Gamma}_2] (\chi_d^R(\omega) - \chi_d^A(\omega)) \\ &\quad + (\tilde{\Gamma}_1 - \tilde{\Gamma}_2) \chi_d^<(\omega)\end{aligned}\quad (\text{C5})$$

where $\tilde{\Gamma}_{1,2} = 2\pi\rho_0 (J_\perp^{(1),(2)})^2$ with ρ_0 being the constant density of states of the leads.

Following Ref. 58, for $\tilde{\Gamma}_1 = \lambda \tilde{\Gamma}_2$, we have

$$\langle \hat{I} \rangle = \int_{-\infty}^{\infty} (f_{\omega-\mu_L} - f_{\omega-\mu_R}) \tilde{\Gamma}(\omega) (\chi_d^R(\omega) - \chi_d^A(\omega)) \quad (\text{C6})$$

where $\tilde{\Gamma}(\omega) = (2\pi\rho_0)^2 \frac{(g_\perp^1(\omega) g_\perp^2(\omega))^2}{(g_\perp^1(\omega))^2 + (g_\perp^2(\omega))^2}$. Note that the Kondo couplings have been generalized to be frequency dependent following the nonequilibrium RG approach.

- ¹ S. Sachdev, *Quantum Phase Transitions*, Cambridge University Press (2000).
- ² S. L. Sondhi, S. M. Girvin, J. P. Carini, and D. Shahar, *Rev. Mod. Phys.* **69**, 315 (1987).
- ³ H. v. Löhneysen, A. Rosch, M. Vojta, and P. Wölfle, *Rev. Mod. Phys.* **79**, 1015 (2007).
- ⁴ I. Safi and H. Saleur, *Phys. Rev. Lett.* **93**, 126602 (2004).
- ⁵ M.H. Devoret, D. Esteve, H. Grabert, G.-L. Ingold, H. Pothier, and C. Urbina, *Phys. Rev. Lett.* **64**, 1824 (1990).
- ⁶ G. Ingold and Yu. V. Nazarov, in *Single Charge Tunneling*, edited by H. Grabert and M. H. Devoret (Plenum Press, New York, 1992).
- ⁷ K. Le Hur, *Phys. Rev. Lett.* **92**, 196804 (2004); M.-R. Li, K. Le Hur, and W. Hofstetter, *Phys. Rev. Lett.* **95**, 086406 (2005).
- ⁸ K. Le Hur and M.-R. Li, *Phys. Rev. B* **72**, 073305 (2005).
- ⁹ L. Borda, G. Zarand, P. Simon, *Phys. Rev. B* **72**, 155311 (2005); L. Borda, G. Zarand, and D. Goldhaber-Gordon, *cond-mat/0602019* (un-published).
- ¹⁰ P. Cedraschi and M. Büttiker, *Annals of Physics (NY)* **289**, 1 (2001).
- ¹¹ A. Furusaki and K. A. Matveev, *Phys. Rev. Lett.* **88**, 226404 (2002).
- ¹² M. Goldstein, Y. Gefen, and R. Berkovits, *Phys. Rev. B* **83**, 245112 (2011).
- ¹³ P. Cedraschi, V. V. Ponomarenko, and M. Büttiker, *Phys. Rev. Lett.* **84**, 346 (2000).
- ¹⁴ G. Zarand, C.H. Chung, P. Simon, and M. Vojta, *Phys. Rev. Lett.* **97**, 166802 (2006).
- ¹⁵ A. Recati, P. O. Fedichev, W. Zwerger, J. von Delft, and P. Zoller, *Phys. Rev. Lett.* **94**, 040404 (2005).
- ¹⁶ C.H. Chung, K. Le Hur, M. Vojta and P. Wölfle, *Phys. Rev. Lett.* **102**, 216803 (2009).
- ¹⁷ C.H. Chung, K.V.P. Latha, K. Le Hur, M. Vojta and P. Wölfle, *Phys. Rev. B*, **82**, 115325 (2010).
- ¹⁸ C.H. Chung and K.V.P. Latha, *Phys. Rev. B* **82**, 085120 (2010).
- ¹⁹ D. E. Feldman, *Phys. Rev. Lett.*, **95**, 177201 (2005).
- ²⁰ A. Mitra, S. Takei, Y.B. Kim, and A. J. Millis, *Phys. Rev. Lett.*, **97**, 236808 (2006).
- ²¹ R. M. Potok, I. G. Rau, H. Shtrikman, Y. Oreg, and D. Goldhaber-Gordon, *Nature* **447**, 167 (2007).
- ²² S. Kirchner, Q.M. Si, *Phys. Rev. Lett.* **103**, 206401 (2009).
- ²³ S. Takei, Y.B. Kim, *Phys. Rev. B* **76** 115304 (2007); S. Takei, W. Witczak-Krempa, Y.B. Kim, *Phys. Rev. B* **81**, 125430 (2010).
- ²⁴ Dittrich, P. Hanggi, G-I. Ingold, B. Kramer and G. Schön, W. Zwerger, *Quantum Transport and Dissipation* (Viley-VCH, 1998).
- ²⁵ S. Florens, P. Simon, S. Andergassen, and D. Feinberg, *Phys. Rev. B* **75**, 155321 (2007).
- ²⁶ J. Schwinger, *J. Math. Phys.* **2**, 407 (1961); L. V. Keldysh, *Soviet Physics JETP* **20**, 1018 (1965); J. Rammer and H. Smith, *Rev. Mod. Phys.* **58**, 323 (1986); A. P. Jauho, N. S. Wingreen and Y. Meir, *Phys. Rev. B* **50**, 5528 (1994).
- ²⁷ A. Rosch J. Paaske, J. Kroha and P. Wölfle, *Phys. Rev. Lett.* **90**, 076804 (2003); A. Rosch, J. Paaske, J. Kroha, P. Wölfle, *J. Phys. Soc. Jpn.* **74**, 118 (2005).
- ²⁸ H. Schoeller, *Eur. Phys. J. Special Topics* **168**, 179 (2009).
- ²⁹ S. Kehrein, *Phys. Rev. Lett.* **95**, 056602 (2005).
- ³⁰ S. G. Jakobs, V. Meden and H. Schoeller, *Phys. Rev. Lett.* **99**, 150603 (2007); C. Karrasch et al., *Phys. Rev. B* **81**, 125122 (2010).
- ³¹ H. Schmidt and P. Wölfle, *Ann. Phys. (Berlin)* **19**, 60 (2010).
- ³² C. Mora, P. Vitushinsky, X. Leyronas, A. A. Clerk, and K. Le Hur, *Phys. Rev. B* **80**, 155322 (2009); P. Vitushinsky, A. A. Clerk, and K. Le Hur, *Phys. Rev. Lett.* **100**, 036603 (2008); C. Mora, X. Leyronas and N. Regnault, *Phys. Rev. Lett.* **100**, 036604 (2008); Z. Ratiani and A. Mitra, *Phys. Rev. B* **79**, 24511 (2009).
- ³³ C. Timm, *Phys. Rev. B* **83**, 115416 (2011).
- ³⁴ P. Fendley, A. W. W. Ludwig and H. Saleur, *Phys. Rev. Lett.* **74**, 3005 (1995).
- ³⁵ P. Mehta and N. Andrei, *Phys. Rev. Lett.* **96**, 216802 (2006); P. Mehta and N. Andrei, *arXiv:0702612* (2007).
- ³⁶ P. Dutt, J. Koch, J.E. Han, K. Le Hur, *Annals of Physics* **326**, 2963 (2011).
- ³⁷ E. Boulat, H. Saleur and P. Schmitteckert, *Phys. Rev. Lett.* **101**, 140601 (2008); F. Heidrich-Meisner, A. E. Feiguin and E. Dagotto, *Phys. Rev. B* **79**, 235336 (2009).
- ³⁸ F. B. Anders, *Phys. Rev. Lett.* **101**, 066804 (2008); S. Schmitt and F.B. Anders, *Phys. Rev. B* **81**, 165106 (2010).
- ³⁹ M. Schiro and M. Fabrizio, *Phys. Rev. B* **79**, 155302 (2009); P. Werner, T. Oka and A. J. Millis, *Phys. Rev. B* **79**, 035320 (2009); T. L. Schmidt, P. Werner, L. Muehlbacher, A. Komnik, *Phys. Rev. B* **78**, 235110 (2008); P. Werner et al., *Phys. Rev. B* **81**, 035108 (2010); L. Muehlbacher, D. F. Urban, and A. Komnik, *Phys. Rev. B* **83**, 075107 (2011); E. Gull, A. J. Millis, A.I. Lichtenstein, A. N. Rubtsov, M. Troyer, and P. Werner, *Rev. Mod. Phys.* **83**, 349 (2011).
- ⁴⁰ J. E. Han and R. J. Heary, *Phys. Rev. Lett.* **99**, 236808 (2007); J. E. Han, *Phys. Rev. B* **81**, 245107 (2010).
- ⁴¹ J. Gilmore and R. H. McKenzie, 2005 *J. Phys.: Condens. Matter* **17**, 1735.
- ⁴² See, for example: A. Feiguin, P. Fendley, M. Fisher, and C. Nayak, *Phys. Rev. Lett.* **101**, 236801 (2008); A. M. Chang, *Rev. Mod. Phys.* **75**, 1449 (2003); M. Grayson, D. C. Tsui, L. N. Pfeiffer, K. W. West, and A. M. Chang, *Phys. Rev. Lett.* **86**, 2645 (2001).
- ⁴³ Y. Bomze, H. Mebrahtu, I. Borzenets, A. Makarovski, and G. Finkelstein, *Phys. Rev. B* **79**, 241402(R) (2009); H. T. Mebrahtu, I. V. Borzenets, D. E. Liu, H. Zheng, Y. V. Bomze, A. I. Smirnov, H. U. Baranger, and G. Finkelstein, *Nature* **488**, 61, (2012).
- ⁴⁴ G. Refael, E. Demler, Y. Oreg, and D. S. Fisher, *Phys. Rev. B* **75**, 014522 (2007).
- ⁴⁵ G. D. Torre, E. Demler, T. Giamarchi, E. Altman, *Nat. Phys.* **6**, 806-810 (2010); E. G. Dalla Torre, E. Demler, T. Giamarchi, E. Altman, *Phys. Rev. B* **85**, 184302 (2012).
- ⁴⁶ A. M. Lobos and T. Giamarchi, *Phys. Rev. B* **84**, 024523 (2011).
- ⁴⁷ N. Mason and A. Kapitulnik, *Phy. Rev. B* **65**, 220505 (2002).
- ⁴⁸ K.-H. Wagenblast, A. van Otterlo, G. Schön, and G. T. Zimányi, *Phys. Rev. Lett.* **78**, 1779 (1997).
- ⁴⁹ A. J. Rimberg, T. R. Ho, C. Kurdak, J. Clarke, K. L. Campman, and A. C. Gossard *Phys. Rev. Lett.* **78**, 2632 (1997).
- ⁵⁰ M.R. Delbecq, V. Schmitt, F.D. Parmentier, N. Roch, J.J. Viennot, G. Féve, B. Huard, C. Mora, A. Cottet and T.

- Kontos, Phys. Rev. Lett. **107**, 256804 (2011); K. D. Petersson *et al.*, Nature **490**, 380 (2012); H. Toida *et al.*, arXiv:1206.074; S. J. Chorley *et al.*, Phys. Rev. Lett. **108**, 036802 (2012); T. Frey *et al.*, Phys. Rev. B **86**, 115303 (2012).
- ⁵¹ O. Astafiev, A.M. Zagoskin, A.A. Abdumalikov Jr., Yu. A. Pashkin, T. Yamamoto, K. Inomata, Y. Nakamura, and J.S. Tsai, Science **327**, 840 (2010); K. Le Hur, Phys. Rev. B **85**, 140506(R) (2012); I.-C. Hoi, C.M. Wilson, G. Johansson, T. Palomaki, B. Peropadre, P. Delsing, Phys. Rev. Lett. **107**, 073601 (2011); M. Goldstein, M. H. Devoret, M. Houzet, L. I. Glazman, arXiv:1208.0319; M. Marthaler, Y. Utsumi, D. S. Golubev, A. Shnirman, and Gerd Schön, Phys. Rev. Lett. **107**, 093901 (2011); P.-Q. Jin, M. Marthaler, J. H. Cole, A. Shnirman, and Gerd Schön, Phys. Rev. B **84**, 035322 (2011); H. Zheng, D. J. Gauthier, and H. U. Baranger, Phys. Rev. A **82**, 063816 (2010); H. Zheng, D. J. Gauthier, and H. U. Baranger, Phys. Rev. A **85**, 043832 (2012); P. Longo, P. Schmitteckert and K. Busch Phys. Rev. Lett. **104**, 023602 (2010); J.-T. Shen and S. Fan, Phys. Rev. Lett. **98**, 153003 (2007); J.-T. Shen and S. Fan, Phys. Rev. A **76**, 062709 (2007); A. LeClair, F. Lesage, S. Lukyanov, and H. Saleur, Phys. Lett. A **235**, 203 (1997); R. Konik and A. LeClair, Phys. Rev. B **58**, 1872 (1998).
- ⁵² J. Gilmore and R. McKenzie, J. Phys. C. **11**, 2965 (1999).
- ⁵³ T. Giamarchi, Quantum Physics in One Dimension (Oxford University Press, Oxford, 2004).
- ⁵⁴ A. O. Gogolin, A. A. Nersesyan, and A. M. Tsvelik, Bosonization and Strongly Correlated Systems (Cambridge University Press, Cambridge, 1998).
- ⁵⁵ Jan von Delft and Herbert Schoeller, Ann. Phys. (Berlin) **7**, 225 (1998).
- ⁵⁶ In the delocalized phase, it would be more judicious to redefine $\Psi \rightarrow (t_1 c_1 + t_2 c_2)/\sqrt{t_1^2 + t_2^2}$, and then bosonize and refermionize to get the fermions with spins⁸, Ψ_σ . For
- $V \ll T_K$: $\Psi_\uparrow^\dagger \Psi_\downarrow \leftarrow 1/\sqrt{t_1^2 + t_2^2}(t_1 c_{L\uparrow}^\dagger c_{R\downarrow} + t_2 c_{R\uparrow}^\dagger c_{L\downarrow})$ and $\Psi_\sigma^\dagger \Psi_\sigma \leftarrow (1/\sqrt{t_1^2 + t_2^2}) \sum_{\alpha=L,R} t_\alpha c_{\alpha\sigma}^\dagger c_{\alpha\sigma}$.
- ⁵⁷ J. Paaske, A. Rosch, J. Kroha, and P. Wölfle, Phys. Rev. B **70**, 155301 (2004); J. Paaske, A. Rosch, P. Wölfle, Phys. Rev. B **69**, 155330 (2004).
- ⁵⁸ N. S. Wingreen and Y. Meir, Phys. Rev. B **49**, 11040 (1994).
- ⁵⁹ L. Saminadayar *et al.*, Phys. Rev. Lett. **79**, 2526 (1997); R. de-Picciotto *et al.*, Nature (London) **389**, 162 (1997).
- ⁶⁰ I. Safi, P. Devillars, and T. Martin, Phys. Rev. Lett. **86**, 4628 (2001); S. Vishveshwara, *ibid* **91**, 196803 (2003); C. Bena and C. Nayak, Phys. Rev. B **73**, 155335 (2006).
- ⁶¹ A. Schiller and S. Hershfield, Phys. Rev. B **58**, 14978 (1998).
- ⁶² T. Korb, F. Reininghaus, H. Schoeller, and J. König, Phys. Rev. B **76**, 165316 (2007).
- ⁶³ P. Moca, G. Zarand, C.H. Chung, P. Simon, Phys. Rev. B **83**, 201303(R) (2011).
- ⁶⁴ I. Safi, arXiv:0908.4382; I. Safi, C. Bena, and A. Crépieux, Phys. Rev. B **78**, 205422 (2008).
- ⁶⁵ The FRG approach for the Kondo couplings $g_{\perp,z}(\omega)$ used here¹⁷ (Eq. (11) and Eq. (36)) is somewhat different from that in Ref. 31: In Ref. 31 the RG scaling equation for pseudofermion self-energy is formulated and is solved self-consistently along with the RG scaling equations for the Kondo couplings. Here, following Ref. 17 and Ref. 27 the pseudofermion self energy is included self-consistently through the decoherence rate $\Gamma(\omega)$ where it is computed via the Fermi-Golden rule within the renormalized perturbation theory. Nevertheless, we have checked that the results on $g_{\perp,z}(\omega)$ via both approaches agree very well.
- ⁶⁶ S. Kirchner and Q. Si, Physica Status Solidi (b), **247**, 631 (2010).
- ⁶⁷ K. Le Hur, Phys. Rev. B **74**, 165104 (2006); K. Le Hur, Phys. Rev. Lett. **95**, 076801 (2005).